DESIGN & MODELLING OF SYMMETRIC AND ASYMMETRIC PLASMONIC NANOGRATINGS FOR CHEMICAL/BIOLOGICAL SENSING

A DISSERTATION

SUBMITTED IN PARTIAL FULFILLMENT OF THE REQUIREMENTS

FOR THE AWARD OF DEGREE

OF

MASTER OF TECHNOLOGY

IN

MICROWAVE AND OPTICAL COMMUNICATION

Submitted by:

Vipul Singh Jalal

2K17/MOC/10

Under the supervision of

DR. YASHNA SHARMA

DEPARTMENT OF ELECTRONICS AND COMMUNICATION ENGINEERING

DELHI TECHNOLOGICAL UNIVERSITY

(Formerly Delhi College of Engineering)

Bawana Road, Delhi-110042

SEPTEMBER, 2019

DELHI TECHNOLOGICAL UNIVERSITY
(Formerly Delhi College of Engineering)
Bawana Road, Delhi-110042

CANDIDATE'S DECLARATION

I, Vipul Singh Jalal, Roll No. 2K17/MOC/10, student of M.Tech (Microwave and Optical Communication), hereby declare that the project Dissertation titled "Design & Modelling of Symmetric and Asymmetric Plasmonic Nanogratings for Chemical/Biological Sensing" which is submitted by me to the department of Electronics and Communication Engineering, Delhi Technological University, Delhi in partial fulfilment of the requirement for the award of the degree of degree of Master of Technology, is original and not copied from any source without proper citation. This work has not previously formed the basis for the award of any Degree, Diploma Associateship, Fellowship or other similar title or recognition.

Place: Delhi VIPUL SINGH JALAL

Date:

DEPARTMENT OF ELECTRONICS AND COMMUNICATION ENGINEERING

DELHI TECHNOLOGICAL UNIVERSITY
(Formerly Delhi College of Engineering)
Bawana Road, Delhi-110042

CERTIFICATE

I hereby certify that the project dissertation titled "Design & Modelling of Symmetric and Asymmetric Plasmonic Nanogratings for Chemical/Biological Sensing" which is submitted by Vipul Singh Jalal, Roll No. 2K17/MOC/10, Department of Electronics and Communication Engineering, Delhi Technological University, Delhi in partial fulfilment of the requirement for the award of the degree of Master of Technology, is a record of the project work carried out by the student under my supervision. To the best of my knowledge this work has not been submitted in part or full for any Degree or Diploma to this University or elsewhere.

Place: Delhi

Date:

DR. YASHNA SHARMA

SUPERVISOR

(Assistant Professor, Department of Electronics and Communication Engineering, Delhi Technological University, Bawana Road, Delhi-110042)

ABSTRACT

When optical frequencies are incident on metal nanostructures with corrugations, such as nanoscale gratings with nanoscale gaps, light is coupled into plasmonic modes in these nanostructures. At certain special wavelengths- called the plasmon resonance wavelengths- light couples most strongly into these nanostructures creating electromagnetic hotspots in the grating gaps. This phenomenon of electromagnetic enhancement due to localized surface plasmons can be exploited to create chemical or biological sensors sensitive to nano-molar concentrations of the analytes. In this project, we aim to explore certain specific designs of nanogratings with nanogaps below 20 nm. Symmetric and asymmetric nanogratings will be modelled and simulated in the wavelength range of 400 nm to 1600 nm by employing Rigorous Coupled Wave Analysis. The reflectance spectra will be calculated 'with' and 'without' a biomolecule layer (different biomolecules will be analysed), and sensitivities will be reported as the shift in wavelength per unit refractive index (nm/RIU). We aim at sensors based on such nanogratings which can be tuned to the wavelength range of choice, and can provide multiple sensing wavelengths thus allowing their usage with multiple lasers.

ACKNOWLEDGEMENT

I would like to thank my thesis advisor Dr. Yashna Sharma of Electronics and Communication Engineering Department at Delhi Technological University. She consistently allowed this paper to be my own work, but steered me in the right the direction whenever she thought I needed it and readily helped whenever there was any query.

I would also like to thank all my family and friends for providing me with unfailing support and continuous encouragement throughout my years of study and through the process of researching and writing this thesis. This accomplishment would not have been possible without them. Thank you.

Date: VIPUL SINGH JALAL

CONTENTS

LIST OF FIGURES

LIST OF TABLES

LIST OF ABBREVIATIONS

LSPR	Localised Surface Plasmon Resonance
RCWA	Rigorous Coupled Wave Analysis
SPR	Surface Plasmon Resonance
MPC	Magneto photonic Crystal
SPP	Surface Plasmon Polariton
MOKE	Magneto Optical Kerr Effect
TKE	Transverse Magneto Optic Kerr Effect
SEF	Sensitivity Enhancement Factor
FDTD	Finite Difference Time Domain
RCWA	Rigorous Coupled Wave Analysis
RI	Refractive Index
RIU	Refractive Index Unit
FOM	Figure of Merit
DNA	Deoxyribonucleic Acid
GNP	Gold Nano Particle
LSP	Localised Surface Plasmon
ODE	Ordinary Differential Equation
SAM	Self Assembled Monolayer
EM	Electro-Magnetic
VS	Versus

CHAPTER 1

INTRODUCTION

In the last few decades, there has been extensive interest in phenomenon which deal with light-matter interaction. One of these phenomenon, which results from the localization of plasmons — which are quanta of plasma oscillation — on metallic nanoparticles, is Localised Surface Plasmon Resonance (LSPR). Although, LSPR and its vivid applications have come to limelight in the last few decades, it has was known and had been implemented since the 4th century A.D. The colours of the Church windows and of the Lycurgus cup were known to be a consequence of mixing small amounts of gold and silver, resulting in nanoparticles being embedded in glass. The light is absorbed and scattered for select regions of the visible spectrum by these nanoparticles, thus resulting in vibrant colours to the spectator's eye.

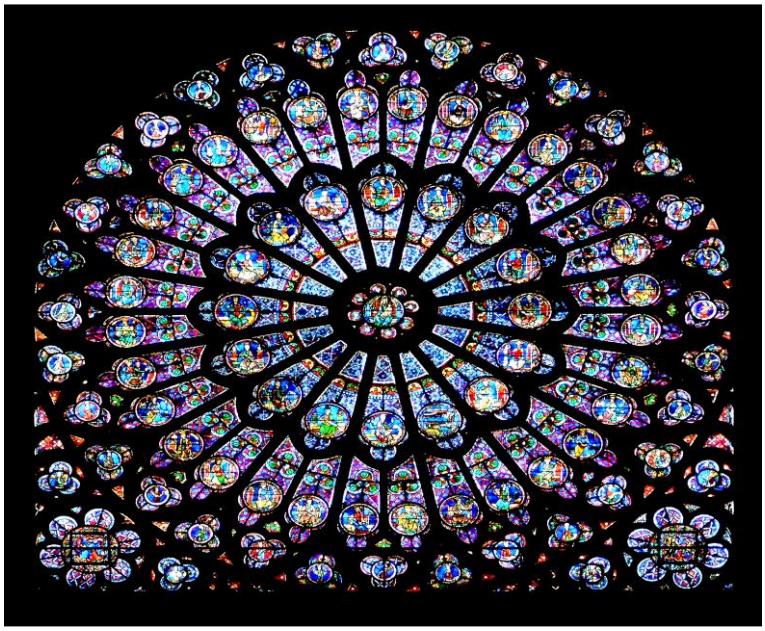

Figure 1.1. Notre-Dame de Paris cathedral has tinted glass window showing colour change due to GNP.

In this work, this phenomenon of LSPR is implemented in order to design a sensor to achieve chemical/ biological sensing. Arrays of symmetric and asymmetric gold nanogratings are exhaustively simulated and the shift in peak wavelengths is studied in order to obtain parameters for an optimised sensor that can be used for sensing

purposes. RCWA (Rigorous Coupled Wave Analysis) method is applied with help of computer simulations in order to calculate the results, and have intended a complete understanding of the electromagnetics behind these results.

The following chapter, chapter 2 gives a brief review of the LSPR phenomenon and elaborates the previous research work carried out in this field, specifically for chemical and biological sensing. A special emphasis has been placed on the literature review of nanogratings and LSPR-based sensors.

As a pre-requisite to the simulations for the complex plasmonic nano-grating structures, symmetric designs were systematically analysed in Chapter 3 to understand the basic physics of coupled plasmonic modes in nanograting employed for this sensing methodology. This is important for the design of more complex, asymmetric designs and for understanding the coupled modes in the complex nanogratings studied in chapter 4. Chapter 4 discusses the effect of integrating differing parameters to form an asymmetric nanogratings, and gives a complete optimization study carried out to obtain higher sensitivity of these sensors.

After optimizing the asymmetric nanograting designs, in Chapter 5, the results of effect of variation of the different grating parameters of the asymmetric nanograting on the sensitivity of these sensors.

CHAPTER 2

LITERRATURE REVIEW

The electron gas clouds present around the nucleus of an atom in a metal oscillate at a certain frequency also known as plasma frequency. When a wave is incident on a metal such that the frequency of the wave is lesser than the plasma frequency, the plasma oscillations form a screen and the incident wave is reflected back. If the frequency of the incident wave is higher than plasma frequency than the plasma oscillations do not have enough time to create a screen and the incident wave is transmitted through the metal. A quantum of plasma oscillations is known as plasmons.

For a particular frequency of the incident wave, all the electrons begin to oscillate coherently. This phenomenon is known as plasmon resonance. The plasmonic resonance can be further divided depending on the origin of oscillations. When the plasmon oscillations are through the volume or bulk of the metal, in such cases occurring resonance are called as bulk plasmon resonance where as for the case when the oscillations are generated at the metal dielectric interface, the plasmons are known as surface plasmons and the resulting plasmonic resonances are termed as surface plasmon resonance (SPR). In the case of nanoparticles with a size much smaller than the incident wavelength, there is a spatial localization of these plasmons around the nanoparticle, thus called- Localized Surface Plasmon Resonance. [1, 2]. This phenomenon of LSPR provides high enhancement to the electromagnetic field and leads to an enhancement in other optical phenomenon such as absorptions and extinction.

Fig. 2.1 shows the schematic diagram for (a) a surface plasmon polariton (propagating plasmon) and (b) a localised surface plasmon [1-3]. Phenomenon of LSPR has been known and studied for quite some time now and as a consequence of the advent of more sophisticated technology and shifting of interest towards newer technologies, new research work has been extensively done involving the principle of LSPR. In the

following section, some of the research work done in previous years has been summarised.

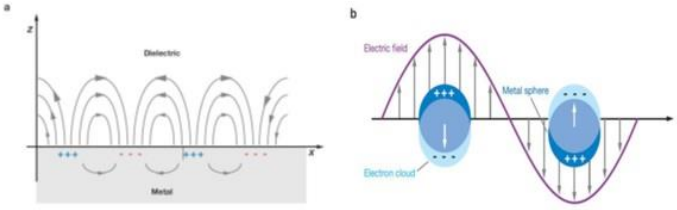

Figure 2.1: (a) Surface plasmon polariton **(b)** Localised surface plasmon.

2.1 SURFACE-PLASMON-INDUCED ENHANCEMENT OF MAGNETO-OPTICAL KERR EFFECT IN ALL-NICKEL SUBWAVELENGTH NANOGRATINGS[4]

A. A. Grunin *et al.*, in 2010, in their work discussed surface-plasmon-induced enhancement of magneto-optical kerr effect in all-nickel subwavelength nanogratings. Magneto photonic crystals (MPCs) are photonic crystals made from transparent magnetic materials find application for enhancing the magneto-optical response [4]. The magnetic material used for practical implementation of a MPC are required to have low absorption in order to ensure considerable photonic-band gap [4]. Surface plasmon polaritons (SPP) are the only phenomena of metals that is found analogous to the effects of photonic band gap [4].

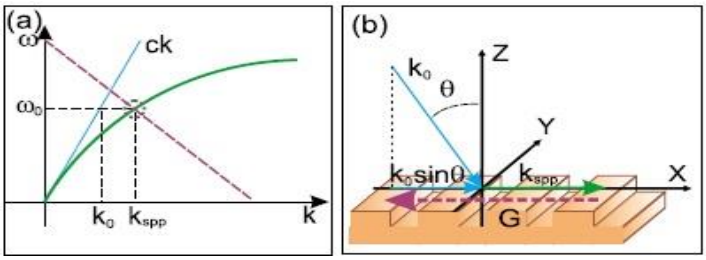

Figure 2.2 (a) SPP phasematching (b) Configuration for setup [4].

Strong modification of magneto-optical response near plasmonic resonances was discussed theoretically in Refs. 5-7. Local plasmon resonance lead to Magneto-optical Kerr effect (MOKE) enhancement in magnetic materials saturated with metallic nanoparticles [8-11]. In this work, a combination of plasmonic and magnetophotonic crystal phenomenons are combined for realisation of effects of magneto-optic Kerr effect [4]. Subwavelength nanostructure of nickel film is implemented in order to reach conditions of phase matching for SPP and enhancement of transversal magneto-optical

Kerr effect (TKE) [4]. The 1D nanograting is periodic with periodicity nearly equal to half of the desired spectral range optical wavelength [4].

The phase match condition for incident wave and the propagating SPP through the metal strips can be given as $k_0 \sin\theta + k_{spp} + nG=0$, where k_0 and k_{spp} are the wave vectors of incident wave and SPP, respectively; G is the reciprocal vector; *n* is the diffraction order; and θ is the angle of incidence[4]. Above condition for phase match is met for subwavelength grating by using -1st diffraction order. Figure 2.2 shows the same [4]. The author varies the angle of incidence and observes the reflection spectra for varying angles and reaches a conclusion that TKE is enhanced to almost 1 degree because of resonant excitation of surface plasmon-polaritons [4].

2.2 EFFECT OF SURFACE PLASMON RESONANCE ON THE OPTICAL ACTIVITY OF CHIRAL METAL NANOGRATINGS [12]

In 2007, K Konishi *et al.*, presented their study on SPR effects on optical response of chiral metal nanogratings. The optical response from a metal nanograting is a result of surface plasmons at the resonant frequency and can be varied by varying the frequency of resonance [12]. In a grating the optical effects arise due to resonant coupling between the photons with small lateral momentum and SP [12]. The resulting optical effects may include either of the following:

- Light transmitted via subwavelength holes is enhanced [13].
- Extinction of light is suppressed [14].
- Various nonlinear and linear optical phenomena [15-17].

The authors have performed numerical and experimental systematic polarization rotation and transmission measurements with different incident angles and sample orientations in order to visualise relationship between surface plasmons and giant optical rotatory power of chiral metal nanogratings and concludes that surface plasmons excited on the air-metal-substrate interfaces of nanostructures play an essential role on the enhancement of optical activity [12].

2.3 LOCALIZED SURFACE PLASMON RESONANCE DETECTION OF LAYERED BIOINTERACTIONS ON METALLIC SUBWAVELENGTH NANOGRATINGS[18]

In 2009, K Kim *et al.*, presented their work, the results of which suggested the feasibility of detecting biomolecular interactions with the help of enhanced LSPR sensitivity and the possibility of a biosensor using LSPR [18]. A label-free, quantitative-based real-time sensing has been implemented by calculating the shift in resonance wavelength which arises in response to interactions between metal nannoparticles [18]. For a traditional thin metal film based SPR biosensor, the sensitivity limit is 1 pg mm^{-2} [19]. Varying approaches proposed in order to enhance the sensitivity of traditional SPR sensors are:

- signal amplification using functionalized nanoparticles [20]
- magneto-optic effects [21]
- surface relief nanostructure-mediated localized SPR (LSPR) [22-25],
- phase -sensitive SPR detection schemes [26,27].

SEF abbrivated for sensitivity enhancement factor is defined as the ratio of resonance angle shift by the target on a nanostructure-based LSPR sample ($\Delta\theta LSPR$) to that on a control sample with no nanostructure ($\Delta\theta control$), i.e. SEF = $\Delta\theta LSPR/\Delta\theta control$, is the parameter used to setup a comparision among the LSPR based viosensor and conventional biosensors [18]. SEF may turn out to be negative due to effect of damping induced by strong index contrast in the dispersion relation and phase retardation by LSP excitation [18]. Negative shift is termed as backbending and was reported in the 1970s [28,29]. In the work done the highest SEF obtained to be 242% for MUA SAM detection using a LSPR biosensor with nanowire of 200 nm periodicity. This SEF is not the absolute highest and can be higher for smaller periods [18].

For the research work done in the paper FDTD and RCWA numerical methods were implemented for numerical determination of designs and the optical setup used in the experiment is as shown in figure

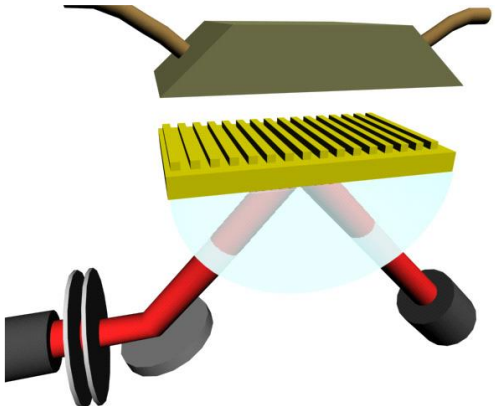

Figure 2.3 Experimental setup schematic [18].

2.4 THE INVESTIGATION OF AN LSPR REFRACTIVE INDEX SENSOR BASED ON PERIODIC GOLD NANORINGS ARRAY[30]

In 2018, Shuai Wang *et al.*, in his work presented a periodic gold nanorings array which works on the principle of LSPR to work as an on-chip refractive index sensor [30]. A RI sensor is constructed with a RI sensitivity of 577 nm/RIU with a FOM of 6.1 [30].

The implemented structure is as shown in fig. 2.4 r_1, r_2 are respectively the inner and outer radii of the cylindrical gold nano structure. Cylinder height is given by h and d representing thickness of cylindrical shell.

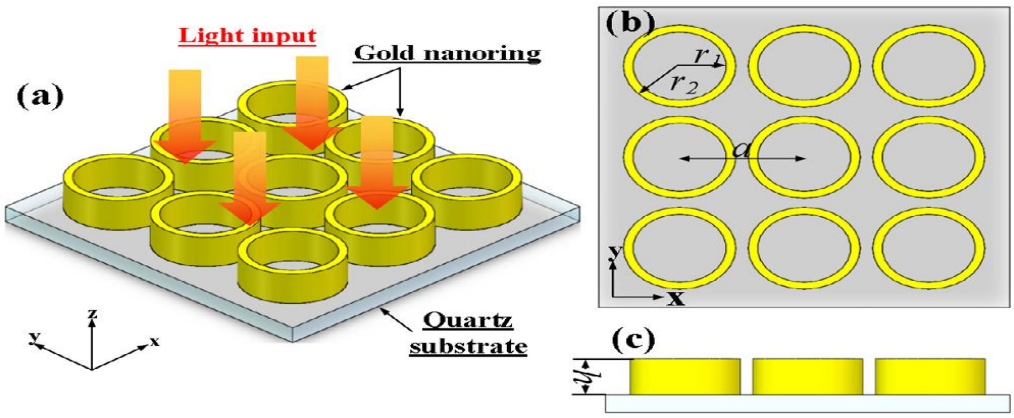

Figure 2.4 Sensor schematic (a) 3D view, (b) top view and (c) side view of the structure [30].

Each of the parameter thickness (d), spacing between structures (a) and height (h) have been varied and the resonant wavelength for varying values of parameters is observed. Exhaustive research was carried in order to obtain optimised values to build an optimised sensor. A resonance peak of 95% at 800nm wavelength when using d= 20nm, a= 140nm and h= 130nm was obtained.

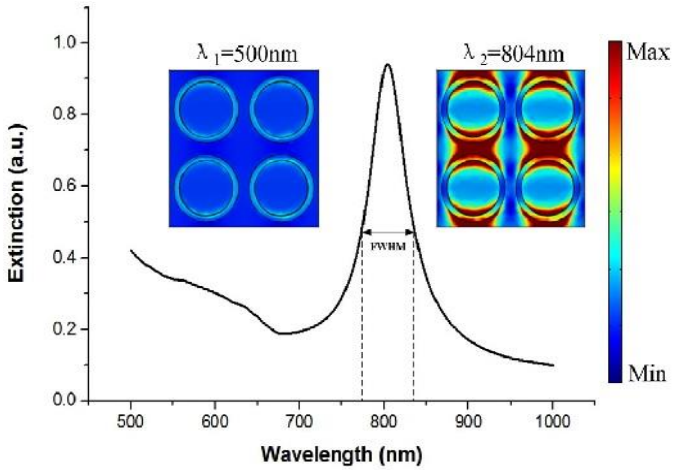

Figure 2.5 Extinction spectra and E field distribution for the structure at 500 nm (off-resonant) and 804 nm (on-resonant) wavelengths.

2.5 LSPR DETECTION OF NUCLEIC ACIDS ON NANOPARTICLE MONOLAYERS[31]

S Thamm *et al.* in 2018 published their work discussing nucleic acid detection via nanoparticle monolayer. Biomolecules binding on the nanoparticle surface lead to a change of the local refractive index, which results in a shift of the peak wavelength [31]. Due to the strong confinement of the electromagnetic field around the nanoparticles surface, high surface sensitivities for small biomolecules can be achieved. The detection of such small biomolecules, here DNA, is based on a specific biomolecule–biomolecule interaction [31].

The capture DNA present on gold nanosphere causes shift in peak wavelength followed by another peak wavelength shift due to hybridisation with complementary DNA. The first step in which the capture DNA is attached to gold nanosphere leads to creation of a biosensor which detects specific molecules. The second step in which the target molecule is attached to the biosensor, leads to successful detection, which can be observed by red shift of the peak wavelength [31].

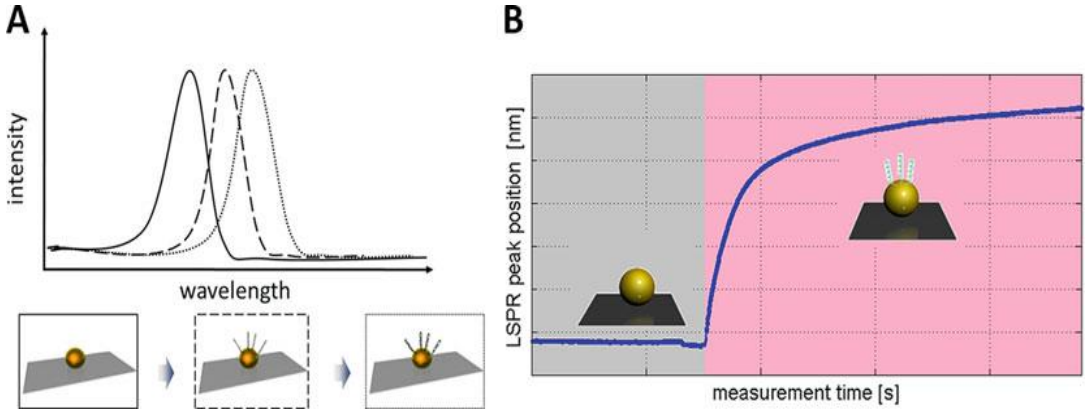

Figure 2.6 (a) Principle of LSPR DNA biosensing. **(b)** Real-time detection of the resonance wavelength shift caused by binding of the capture DNA on the particle surface [31]

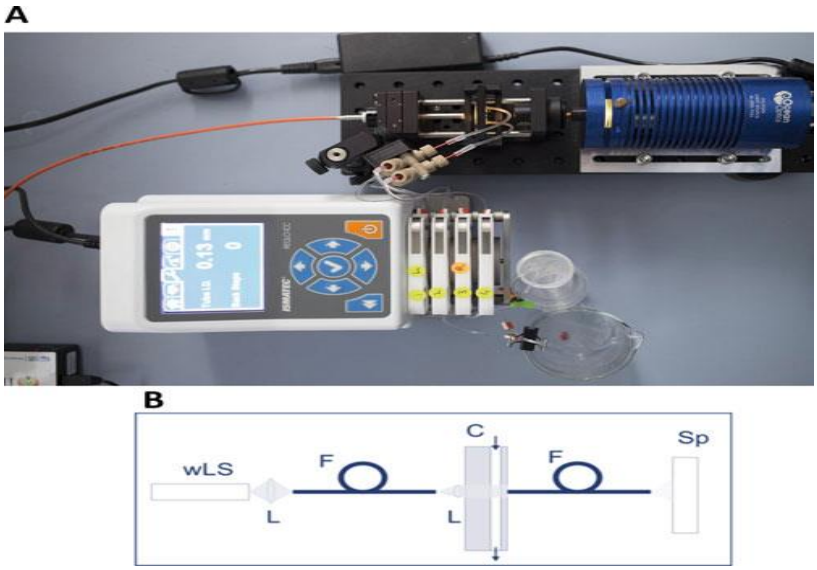

Figure 2.7 (a) EnsLSPR setup **(b)** Measurement setup [31]

Fig. 2.7 shows ensLSPR, i.e. ensemble of nanoparticles, the measurement setup. The detection of nucleic acids is done in several steps, firstly the glass slides are thoroughly cleaned followed by wet chemical silanization in order to increase the affinity of the GNP to the glass surface, so the glass slides are functionalized with amine groups [31]. This is followed by immobilization of the gold nanoparticlesand after the previously mentioned steps are completed, LSPR based is ready for DNA detection [31].

2.6 COLOCALIZATION OF GOLD NANOPARTICLE-CONJUGATED DNA HYBRIDIZATION FOR ENHANCED SURFACE PLASMON DETECTION USING NANOGRATING ANTENNAS [32]

In 2007, Campbell C T and Kim G, in his work showed that the sensing limit for traditional SPR sensors is 1 pg/mm^2 [19]. In order to improve this sensing limit, several

approaches have been taken and using field localization via surface modulation has been found to be more successful in comparision to traditional thin-film-based detection as the fields are not localised in the lateral plane in case of the later [32-33, 18]. Similarly, in order to achieve significant improvement in detection sensitivity, spatial management of biomolecular interaction in the localized evanescent fields has been reported [34, 35].

It is assumed that introducing gold nanoparticles (GNP) to colocalized target molecules would lead to molecular amplification [32]. This in turn would lead to considerable enhancement of detection sensibility obtainable by colocalization without conjugation [32]. The aim of this study is to investigate the achievable sensitivity limit of SPR detection. This is achieved by colocalizing nanoparticle conjugated DNA hybridization and exciting the nanoscale hotspots from nanoantennas [32].

The setup used for the study is as shown in the fig. 2.8. At the side of nanograting ridges small opening to the metal leads to formation of hotspots. The hotspots are created as DNA molecules prefer binding to the metal surface [36], leading to colocalization of DNA hybridisation [32].

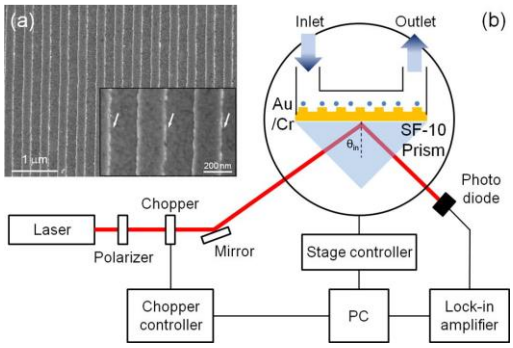

Figure 2.8 (a) SEM images of the fabricated nanograting antenna sample for colocalization of target molecules and near-fields. (b) Experimental configuration. [32]

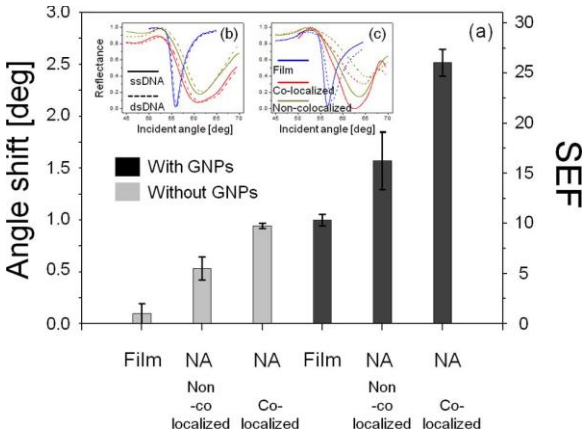

Figure 2.9 (a) SPR shifts and SEF measured for various. Insets present SPR curves, **(b)** with no GNPs (left) and **(c)** with GNPs (right). [32]

An exhaustive study was carried out with varying nanograting depths, periodicity, angle of incidence and the comparative results were drawn out and a distinct conclusion can be made from fig. 2.9 [32]. Concludingly, a near-field hot spots is created using nanograting antenna and colocalized GNP conjugated target molecules with the hot spots [32]. The results show an enhancement by 2 orders of magnitude in the effective index signature and a higher enhancement may be possible by increasing the GNP concentration [32].

2.7 SURFACE-ENHANCED PLASMON RESONANCE DETECTION OF NANOPARTICLE-CONJUGATED DNA HYBRIDIZATION[33]

C. T. Campbell, J. Homola et al. in their works conclude that the traditional thin film based SPR biosensor have a sensitivity limit of order 1 pg/mm^2 [19, 37]. Varying techniques have already been discussed in the sections 2.3 and section 2.6.

S Moon at el. in 2018 in their work experimentally study the merger of two techniques which are firstly the resonance shift due to particle plasmons at the resonance wavelengths at the resonance wavelength [38] and the second being the field enhancements being caused by the localised surface plasmons (LSP) at the local hotspots [33]. Use of long grating structures and nanoparticles were implemented at the same time [39] and the reflectance changes in higher order diffractions are measured [33]. Each of the nanograting wire can be considered to be interacting with the nanoparticles individually and the larger grating pitches prevent the LSP couplings [33].

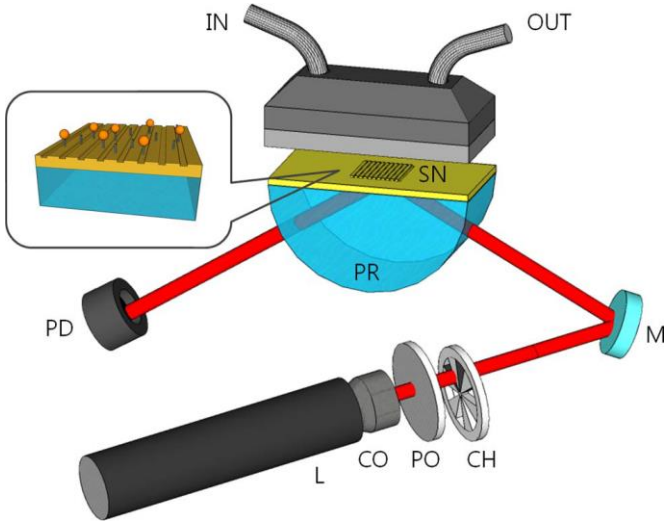

Figure 2.10 Schematics of implemented structure [33].

Fig. 2.10 shows the experimental setup employed in order to obtain various readings where SN is for surface nanograting; M for mirror; PR for prism; CH for chopper; PO for polarizer; CO for collimator; L for light source; PD for photodiode; IN, inlet and OUT stands for outlet. The nanograting structure is employed due to convenience in modelling and fabrication [33]. It is assumed that overall developments are same for all the sub wavelengths structures. Enhancement of overall plasmonic sensitivity is studied quantitatively by employing surface enhancement factor (SEF). SEF is defined as:

$$SEF = \frac{\Delta\theta_{np+sn}}{\Delta\theta}$$

$$= \frac{\Delta\theta_{sn}}{\Delta\theta} \times \frac{\Delta\theta_{np+sn}}{\Delta\theta_{sn}} = SEF_{sn} \cdot SEF_{np} \qquad (1)$$

$\Delta\theta$ denotes resonance angle shift, sn and np denotes SEF associated with surface nanogratings and nanoparticles.

In the study, numerous observations were studied by varying the parameters such as diameter of the nanoparticles, periodicity of the nanogratings resulting resonance shifts were calculated [33]. Overall sensitivity enhancement was found to be exceeding 18 times [33]. Although nanoparticle associated enhancement was precedent in the experimental conditions, an additional 57% enhancement was produced by the surface nanograting and it is also concluded that sensitivity enhancement is linearly related to nanoparticle volume [33].

2.8 SURFACE ENHANCED LOCALIZED SURFACE PLASMON RESONANCE BIOSENSING OF AVIAN INFLUENZA DNA HYBRIDIZATION USING SUBWAVELENGTH METALLIC NANOARRAYS [40]

In 2010, S A Kim *et al.* presented their work discussing LSPR biosensing. SPR biosensors have inherent advantages as them being rapid, quantitative and label free detection [37, 41]. It is because of this, they find wide utility in protein-protein, antigen-antibody and various other biological interactive detections. However, since thin film based biosensors have sensitivity limitations, it is difficult to utilise them in areas of low concentration [42] and therefore other means for enhanced sensitivity have been introduced [20,21,42,43]. The approach taken in this work in order to improve the sensitivity limitation is to build a subwavelength gold nano-arrays on a thin gold film. Nanogratings

and nanoholes with a period of 200 nm were fabricated by electron-beam lithography. The designed structure is used for avian influenza DNA hybridization detection [40].

Field enhancements were calculated using FDTD and a SEF of 2.54 was obtained for grating with periodicity of 200 nm [40]. This improvement is attributed to an increased surface reaction area and stronger coupling between target analytes and excited LSPs supported by the nanohole arrays [40].

2.9 SURFACE PLASMON RESONANCE IN NANOSTRUCTURED METAL FILMS UNDER THE KRETSCHMANN CONFIGURATION[44]

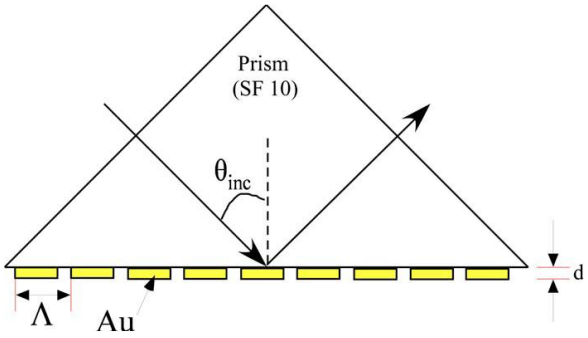

Figure 2.11 The Kretschmann configuration [44].

Hai-Sheng Leong et al., in 2009 published their work in which they discussed SPR in Kretschmann configuration [44]. They calculated the transmittance, reflectance, and absorption [44]. The calculations were made for various periodicity, film thick ness and dielectric fill factor. Kretschmann configuration used in the study is as shown in fig. 2.11 where ∧ is for the periodicity of the nanostructured gratings and d represents thickness of nanostructured film [44].

The SPR angle was found to be reduced and shifted towards the critical angle due to the increased intrinsic free electron oscillation frequency in metal nanostructures and the increase in spatial frequency of the 1D nanograting reduces the surface plasmon resonance angle, which indicates that less momentum is needed to match the momentum of the surface plasmon-polariton [44].

2.10 RIGOROUS COUPLED-WAVE ANALYSIS OF SURFACE PLASMON ENHANCEMENT FROM PATTERNED IMMOBILIZATION ON NANOGRATINGS[48]

Xuyen D. Hoa et al. in this work evaluated the optical response of a Kretschmann SPR biosensor featuring metallic nanogratings and patterned immobilization of surface receptors and parameters are chosen such that the biosensor is operated near the generated bandgap of the surface plasmon dispersion [48]. In the past decades, much research towards sensitivity improvements has been going and it has led to development of novel surface functionalization techniques including nanocolloidal particles, polymer matrices and self-assembled monolayers [48-53].

In this work, unlike grating-coupled SPR [54] and localized SPR spectroscopy [55, 56], in the presented configuration, the coupling to the plasmon mode is achieved via a dielectric prism in a traditional setup and it was concluded that the targeted immobilization of surface receptors onto the nanostructured bio interface of a surface plasmon-based biosensor, in a Kretschmann configuration, can increase the detection sensitivity also allows the concentration of the index change (surface adsorption) to be targeted to zones of high field intensity generated by the grating[48].

2.11 INFLUENCE OF FILM THICKNESS AND NANOGRATING PERIOD ON COLOR-FILTER BEHAVIORS OF PLASMONIC METAL AG FILMS [57]

In 2014 X L Hu *et al.*in their work present the effect of nanograting thickness and period on plasmonic sensors. Colour filters fabricated by sub-micrometers patterning on plasmonic metals thin film are key components for displays, image sensors, digital photography, projectors, and other optical measurement instrumentation [57-63] but the potential applications are held back due to transmission efficiency being less than 60%. Thus the improvement for this is highly demanded. It is fact that the colour filter property strongly depends on patterned microstructure. So, in this work, X. L. Hu et al. carries out a theoretical study for thickness and nanograting period dependences of color filter properties for metal silver (Ag) films from 10nm to 50nm using various sub-micrometer patterns [57]. The design specification of the structure under study is as given in fig. 2.12.

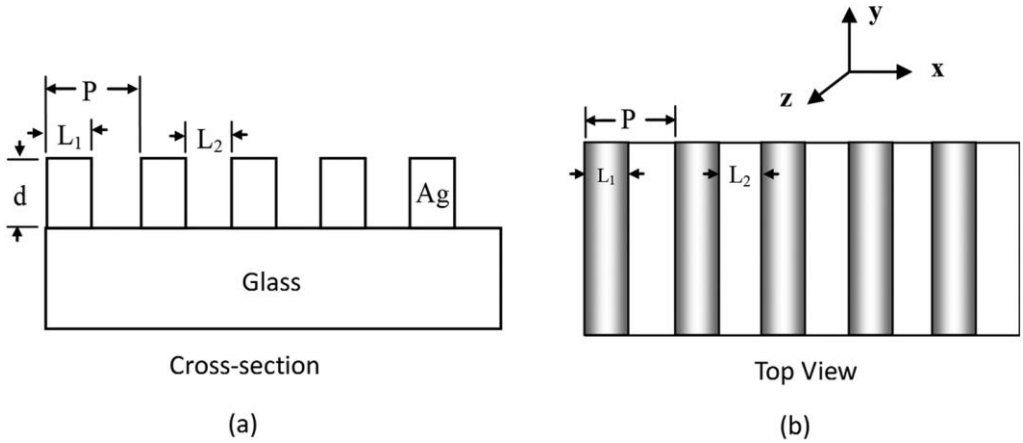

Figure 2.12 Nanograting structure **(a)** Cross-section and **(b)** top view [57].

In this work, $L_1=L_2= P/2$ and P is the period from 220nm to 360nm in a step of 10 nm, *d* is the thickness of metallic Ag film from 15 nm to 50 nm in a step of 5 nm[57]. The author using FDTD solutions, a commercial simulation software, leads to conclusive result as shown in fig. 2.13 and based on the results arrives at the following relationship between the wavelength of transmission minima, grating period and grating thickness [57]:

$$\lambda_{min} = C_0+C_1d+C_2d^2+C_3d^3+C_4P+C_5P^2$$

Here C_i (i = 0-5) are fitting constants with C0=752.1 nm, C1=22.07, C2=0.4273 nm^{-1}, C3=0.002961 nm^{-2}, C4=0.2333, and C5=0.0011 nm^{-1}. This equation is able to predict the transmission minima for a given thickness and period in one-dimensional Ag metallic film nanograting device on glass substrate, revealing its capacity to design color filter device with desirable wavelength [57].

CHAPTER 3

SYMMETRIC NANO-GRATINGS AS PLASMONIC SENSORS

It has been established through previous research that thin film nanosensors reach a sensitivity limit of 1 pg/mm^2 [19, 37]. In the last few decades, various methods have been proposed and researched upon in order to increase this limit. One of the method that has come out is the use of plasmonic nanogratings which helps in increasing the sensitivity limit for multiple reasons. It leads to the confinement of plasmons due to narrow grating widths which lead to a high confinement of electromagnetic energy. Moreover, the coupling of light to plasmons in such nanogratings is easier as no complex prism coupling mechanisms are required. In this research work, gold nanograting structures have been chosen as our focus as gold is chemically more stable than silver or other plasmonic metals.

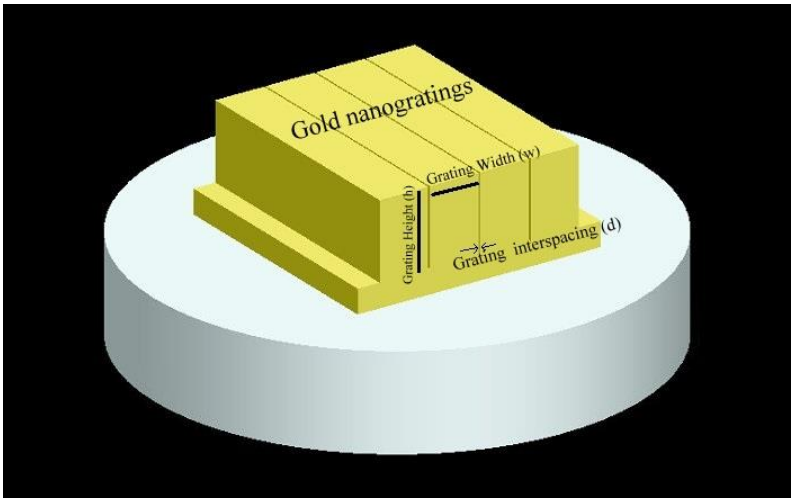

Figure 3.1 Layout for the symmetric gold nanograting.

Our end objective is to design a plasmonic sensor that provides good sensitivity along with the possibility of sensing at multiple plasmon resonance wavelengths. In order find the optimized nano-grating structure, reflectance vs wavelength graphs for various geometrical parameters of such symmetric gratings are obtained by employing Rigorous Coupled Wave Analysis (RCWA). RCWA is a method for numerical modeling of the diffraction of electromagnetic waves on periodic gratings. In the most basic 2D form, RCWA assumes the form of a very simple rectangular gratings. The simple rectangular

form of a grating allows in RCWA an easy separation of space variables, and, using Fourier expansions for the space periodic part of the solution, a transformation of the problem described by the partial differential equations into the system of ordinary differential equations (ODE) for the Fourier amplitudes. The parameters being varied are grating interspacing (basically keeping the grating width constant and varying the periodicity) and the grating heights. Fig. 3.1 shows the layout for the symmetric nanogratings based sensor along with various geometrical parameters.

The working of the sensor is depicted in fig. 3.2. It is a three step process, firstly a capture biomolecule is introduced to the sensor (fig. 3.2.a) which is complementary to the target biomolecule. Introducing the capture biomolecule leads to the formation of a Self Assembled Monolayer (SAM). When the target DNA comes in contact to sensor, it leads to a hybridisation of molecules (fig. 3.2.c), as a consequence of which the refractive index of is altered. This change in the property of the material effects the conditions at which incident light coupled into the plasmonic modes of the nanograting, thus leading to a shift in the resonance wavelength. The shift could either be a red shift or a blue shift. A red shift here represents that the resonance condition is achieved at a higher wavelength or at a lower energy. Similarly, a blue shift denotes a lower resonance wavelength (higher energy state).

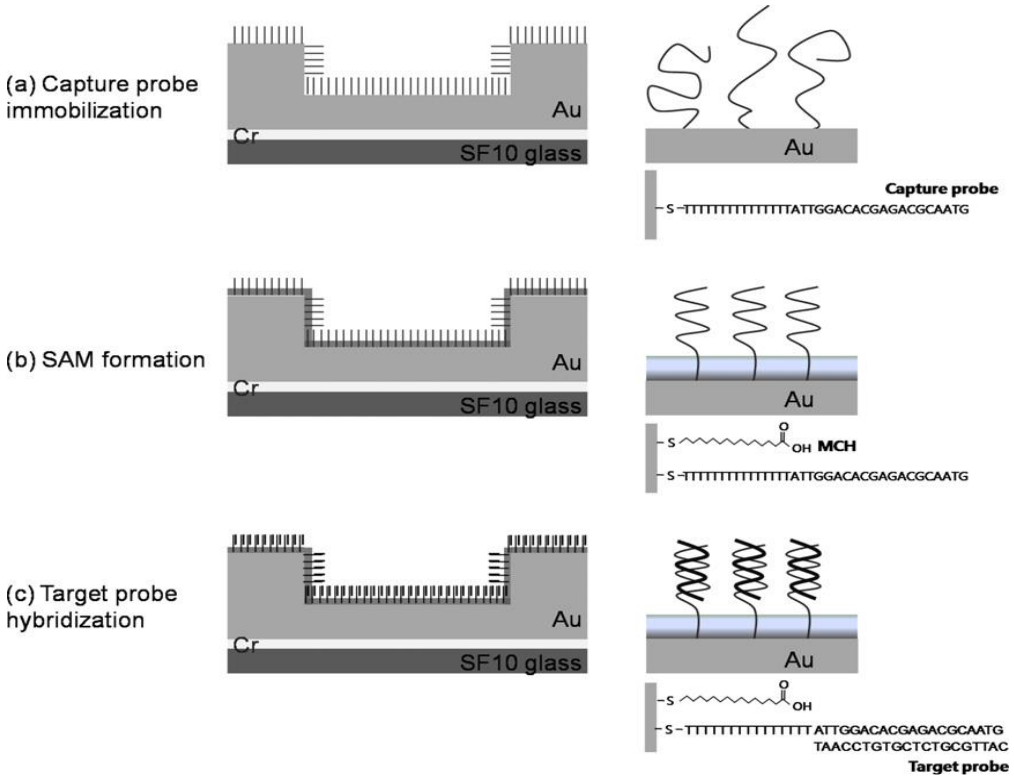

Figure 3.2 Illustration of capture immobilization, MCH treatment and target AI-DNA hybridization on an LSPR sensor chip. [40]

The sensitivity of such a sensor is measured by the change in resonance wavelength per refractive index unit. The amount of resonance wavelength shift is effected by the structure of the sensor. Therefore, in order to design an optimal sensor, the geometrical parameters such as the grating interspacing (*d*) and the grating height (*h*) must be varied one at a time while keeping the other constant. For all such combinations, the diffraction efficiency curves are obtained and the shift in the plasmon resonance wavelength is tabulated.

We begin our work with the symmetric gratings where the individual grating height or width or interspacing are equal throughout the grating structure. In this section the work done has been categorised into (a) Narrow Gap Regime and (b) Wide Gap Regime. The term narrow gap regime implies the fact that the inter-grating spacing between two adjacent gratings is very small. In this work, the maximum grating spacing in this regime is taken as 20 nm, the minimum grating gap is taken as 2 nm in this design. The simulation designs do not go lower than 2 nm due to technological constrains in fabricating structures nearing 1 nm precision. Similarly, for wide gap regime the inter-grating spacing has been constrained to a minimum of 60 nm and upto a maximum of 200 nm grating spacing have been considered in the designs.

3.1 NARROW GAP REGIME

It is an established fact that the closer the nanoparticles are, the higher is the field enhancement obtained. For this reason, our main focus of interest for not only this section but further along the way shall remain the narrow gap regime. In the narrow gap regime, the structures shall haiive inter-grating spacing (*d*) not exceeding 20 nm. Furthermore, to study the magnitude of sensitivity offered by these structures, the nanogratings are simulated without and with a biomolecule layer with a refractive index 1.58. The target biomolecule refractive index is taken 1.58 as it is the refractive index for nucleic acid bio molecules. The work done here requires the variation of dimensions of the nanograting to design a biosensor with optimised dimensionality. It is understood that on increasing the grating widths, the area available for EM absorption and enhancement is increased but if grating widths are increased much higher, the mie scattering is introduced in structure. Although this might increase in number of observable dips but the focus is on LSPR, therefore the grating widths are taken to be 60 nm. The following two cases are studied:

3.1.1 Effect of varying the grating interspacing (*d*)

The sensor structure is made such that a 50 nm thin gold film is used over an underlying substrate and grating structures are built over it. In this section grating height has been kept constant and grating interspacing (*d*) is varied from 2 nm to 20 nm with step size. The grating height is taken to be 150 nm and the gratings are 60 nm wide. A graph of diffraction efficiency vs wavelength is plotted which is as shown in fig. 3.3 and fig. 3.4.

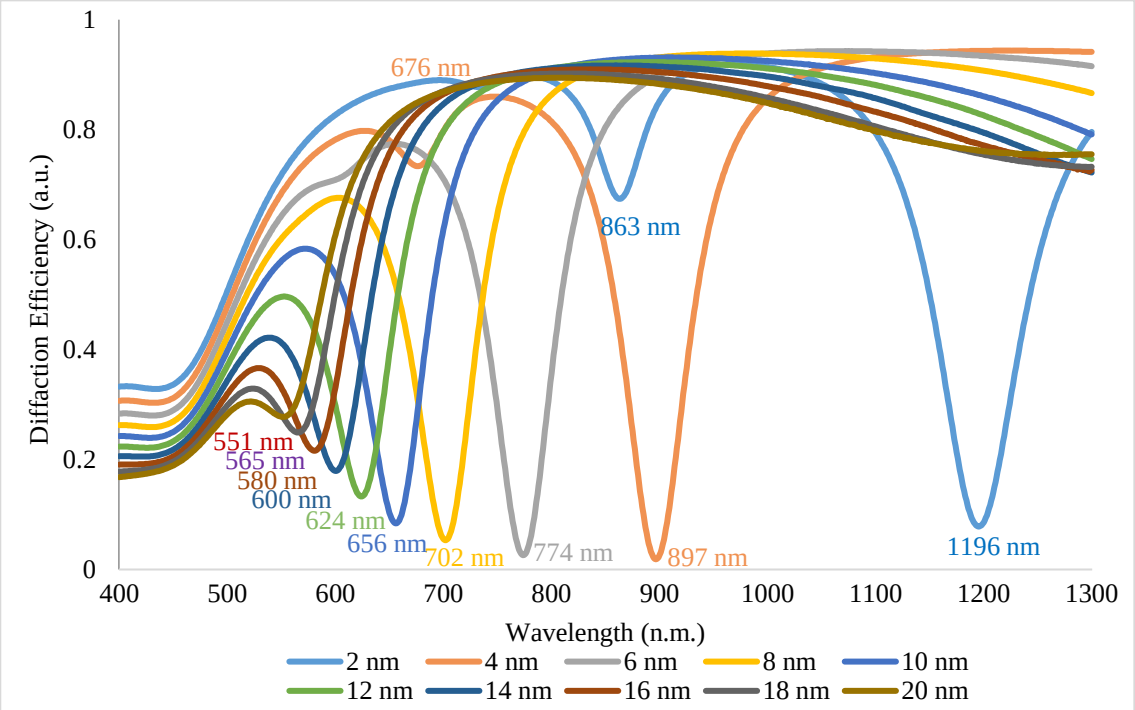

Figure 3.3 Diffraction efficiency VS wavelength curve with varying grating spacing

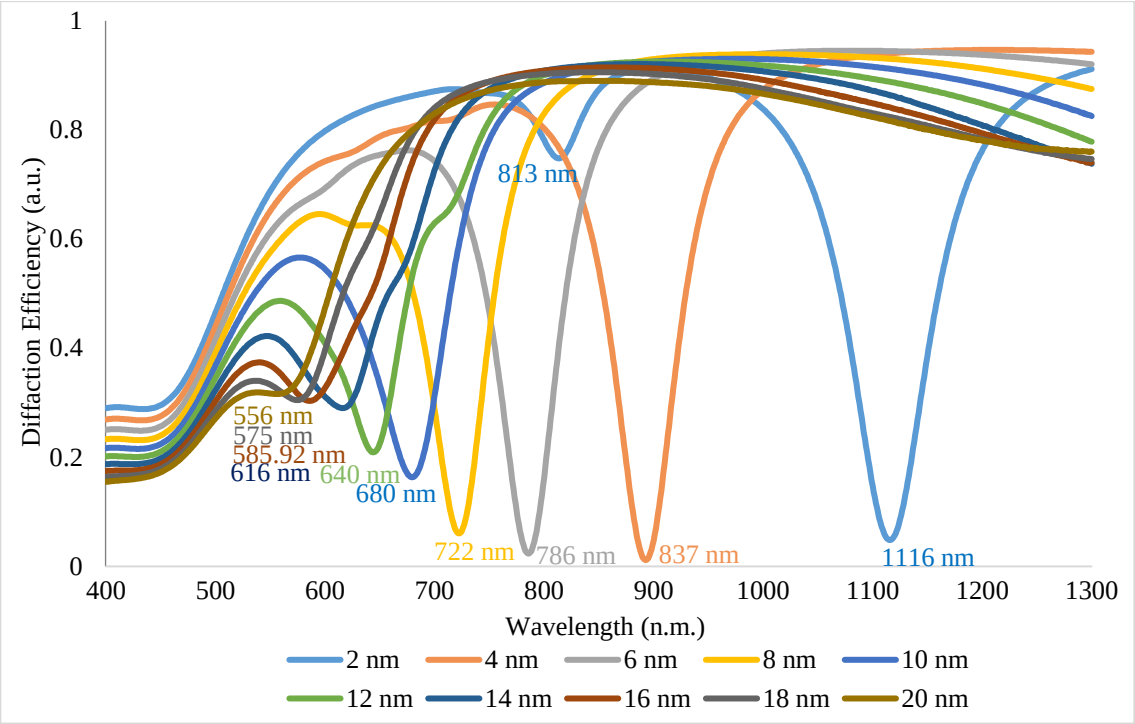

Figure 3.4 Diffraction efficiency VS wavelength curve in presence of target biomolecule

It is observed from fig. 3.4 that with increase in the inter-grating distance, resonance wavelengths are blue shifted, that is the resonance now occurs at smaller wavelengths and higher energy is required to achieve it. One other thing that can also be interpreted is, decreasing the *h*:*d* ratio leads to a higher amount of energy being required for the resonance. Data for resonance dips from fig. 3.3 and fig. 3.4 has been tabulated in Table 3.1

Table 3.1 Comparison for shift in wavelengths for various grating interspacings.

Grating Interspacing (d) (nm)	**Without biomolecule (nm)**		**With biomolecule (nm)**		**Shift (nm)**	
	Dip 1	**Dip 2**	**Dip 1**	**Dip 2**	**1**	**2**
2	863	1196	813	1116	-50	-80
4	676	897	null	893	null	-4
6	null	774	null	786	null	12
8	null	702	null	722	null	20
10	null	656	null	680	null	24
12	null	624	null	644	null	20
14	null	600	null	616	null	16
16	null	580	null	585.92	null	5.92
18	null	565	null	575	null	10
20	null	551	null	556	null	5

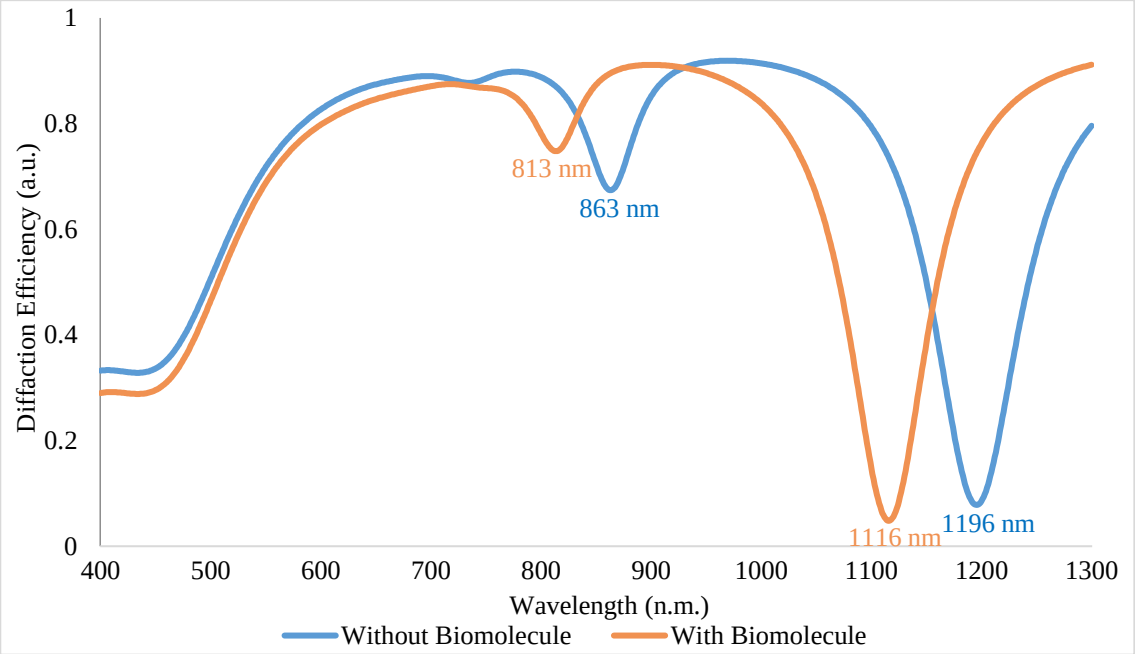

Figure 3.5 Comparison curves for 2 nm grating space

As is seen from the table 3.1, in case of 2 nm grating interspacing, apart from two wavelengths for plasmonic resonance, observed shift in resonant wavelength is also quite significant for both resonance points. The addition of another resonant wavelength is of great significance as it provides us with additional flexibility to use lasers of either wavelengths for sensing. Also since the shift in resonance wavelength is quite significant, it signifies increased sensitivity.

The resonance wavelengths for 2 nm grating spacing are blue shifted at both resonances and it can be distinctly observed from following fig. 3.5

3.1.2 Effect of varying grating height (*h*)

In the previous section, on altering grating spacing it was observed that the best result is attained for 2 nm grating, therefore in this section the inter-grating spacing is kept constant and is equal to 2 nm. Although difficult to fabricate, these nanograting widths can be fabricated by newer lithographic technologies such as multi-step E Beam Lithography. The grating width is taken constant at w = 60 nm and the grating heights are varied from 50 nm to 250 nm in steps of 50 nm. The diffraction efficiency vs wavelength curve for above specifications is plotted which is as shown in fig. 3.6

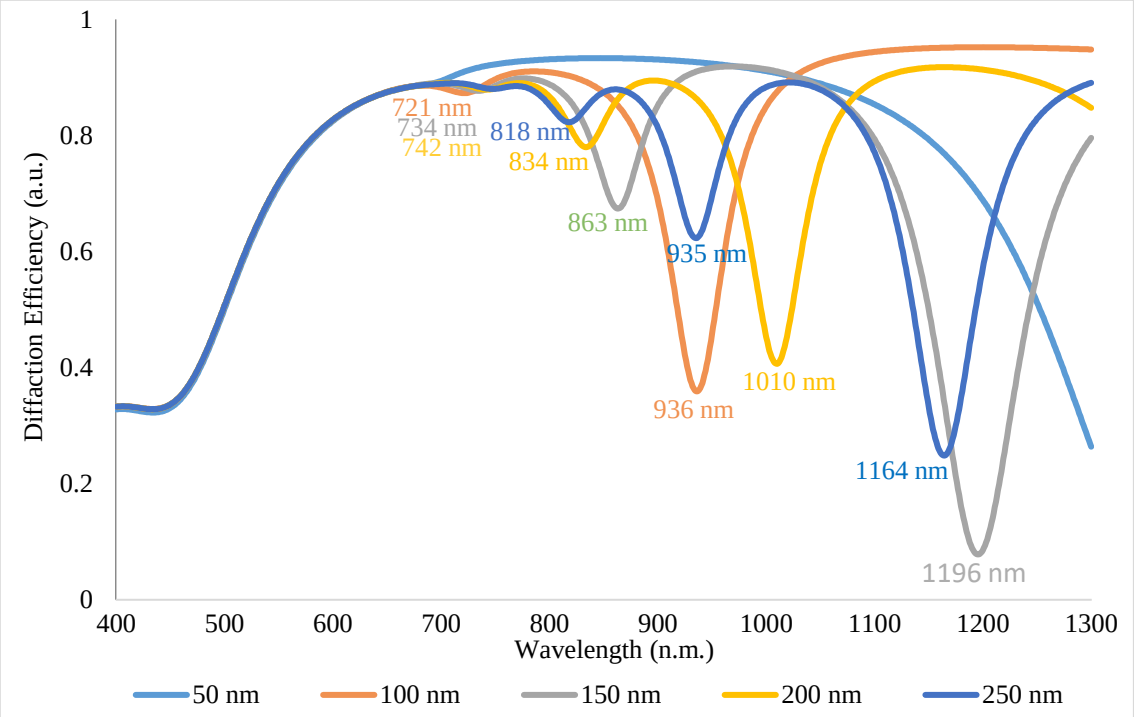

Figure 3.6 Diffraction efficiency VS wavelength curve with varying heights

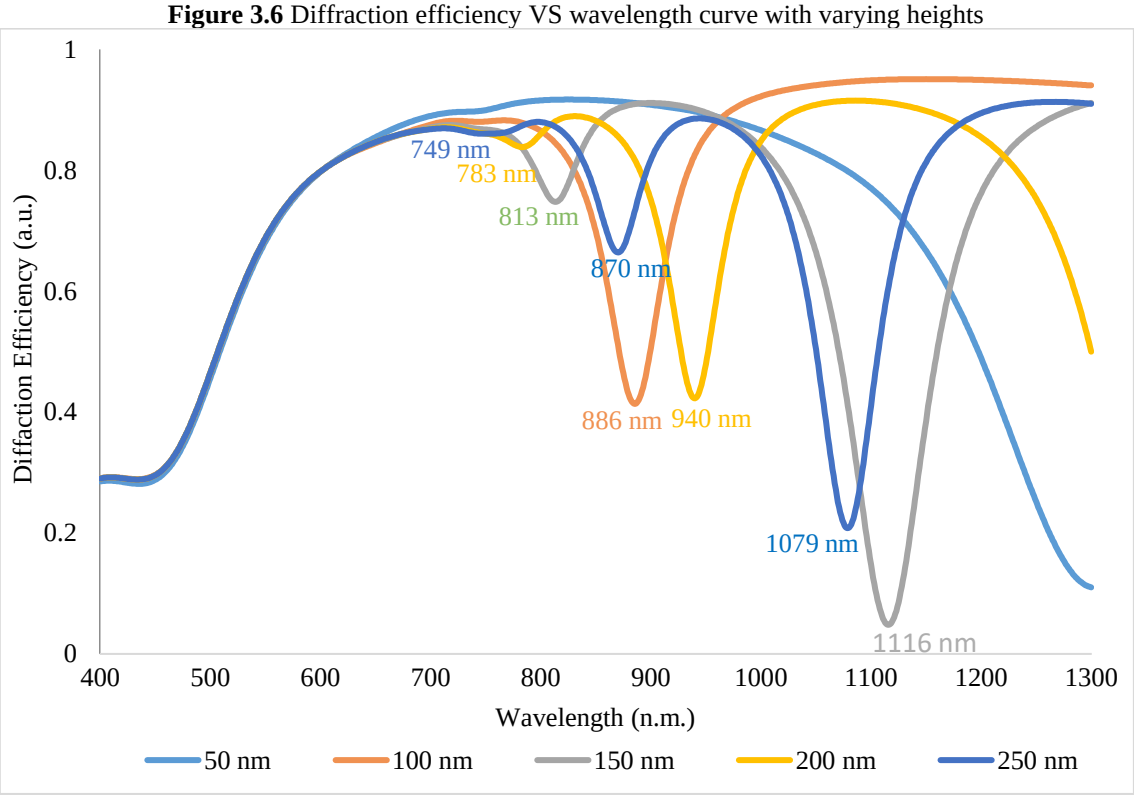

Figure 3.7 Diffraction efficiency VS wavelength curve in presence of target biomolecule

From the previous graphs it is observed that in the presence of target molecule, all the resonance wavelengths are blue shifted. It is also observed that as the grating height is increased multiple wavelengths for resonance are attained. This also serves to verify the

claim from previous section that higher value of *h*:*d* ratio leads to better results. Observations from above graphs are tabulated in the following table.

Table 3.2 Comparison for shift in wavelengths for various grating interspacings.

Grating Height (nm)	**Without biomolecule (nm)**			**With biomolecule (nm)**			**Shift (nm)**		
	Dip 1	**Dip 2**	**Dip 3**	**Dip 1**	**Dip 2**	**Dip 3**	**1**	**2**	**3**
50	null	null	null	null	null	null	null	null	null
100	null	721	936	null	null	886	null	null	-50
150	734	863	1196	null	813	1116	null	-50	-80
200	742	834	1010	null	783	940	null	-51	-70
250	818	935	1164	749	870	1079	-69	-65	-85

It is also observed from above comparisons that although highest points of resonance are observed for 250 nm grating height, least reflectance is observed fir the case of 150 nm height. Fig. 3.8 gives much clearer comparison when studying the resonance wavelength shift for this case. It can be seen that all three resonance points show a significant blue shift not less 65 nm in any of the cases.

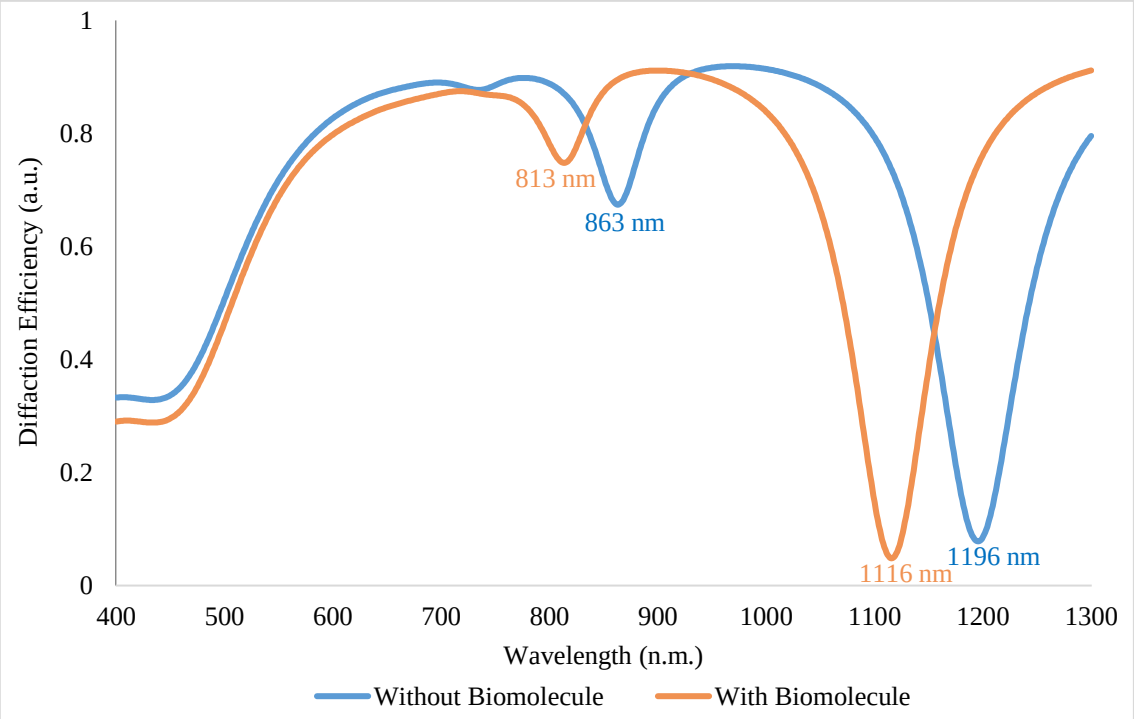

Figure 3.8 Comparison curves for 250 nm grating height

3.2 WIDE GAP REGIME

The main subject of interest for the work here, as has been discussed in the previous section is narrow gap regime, but in order to reaffirm our approach the previously discussed cases are studied for the wide gap regime too. These structures are classified under wide gap regime for the grating gap is 60 nm or higher. Similar to the previous section, section 3.1 structures are studied under two sub sections, in each of which either grating gap or grating height are taken to be constant.

For this regime, the grating widths are taken to be 500 nm. Since coupling of incident light to plasmonic modes with these grating gaps are generally negligible, this study was aimed only at a basic electromagnetic study of such structures. The gratings structures are studied at a height of 150 nm. Furthermore for each sub section there are two cases, firstly diffraction efficiency VS wavelength curves for the sensor only followed by when sensor is in acquisition of the target molecule. In order to emulate target capture conditions we, use a layer of biomolecule with refractive index of 1.58 for our simulations.

3.2.1 Effect of varying the grating interspacing (*d*)

Similar to previous sensor designs, the sensor structure is made such that a 50 nm thin gold film is used and grating structures are built over it. In this section grating interspacing is varied while the grating width and height are kept constant. The grating height is taken to be 150nm and the gratings are 500nm wide. The interspacing (*d*) is varied from 60 nm to 200nm with step size of 20nm and a graph of diffraction efficiency vs wavelength is plotted which is as shown in fig. 3.9.

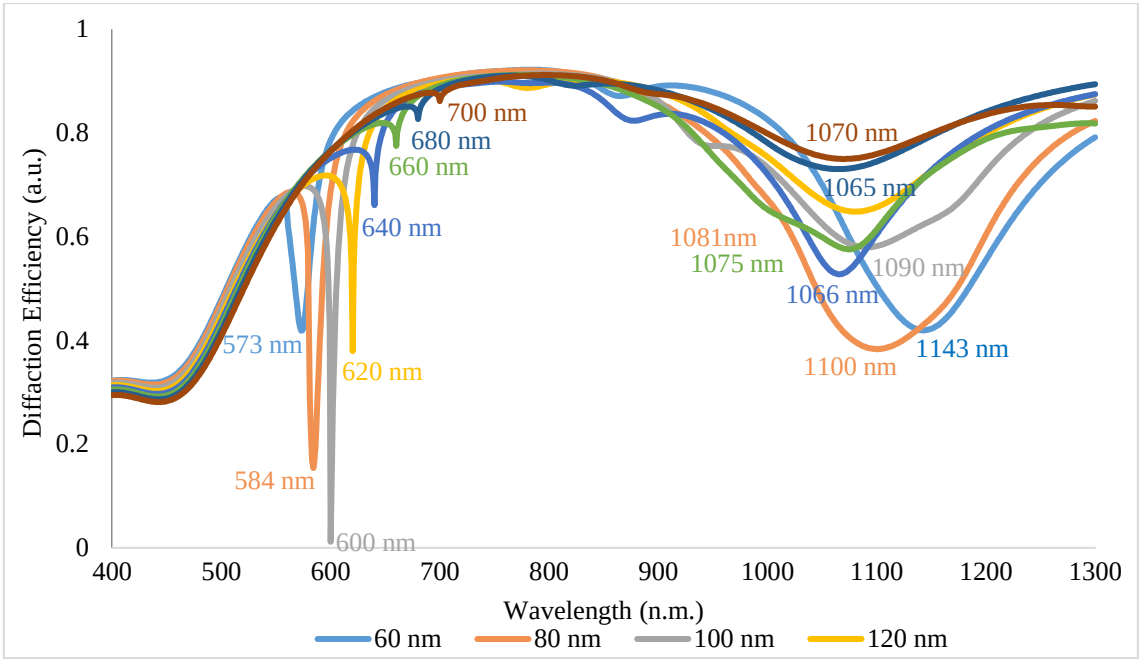

Figure 3.9 Diffraction efficiency VS wavelength curve with varying grating spacing

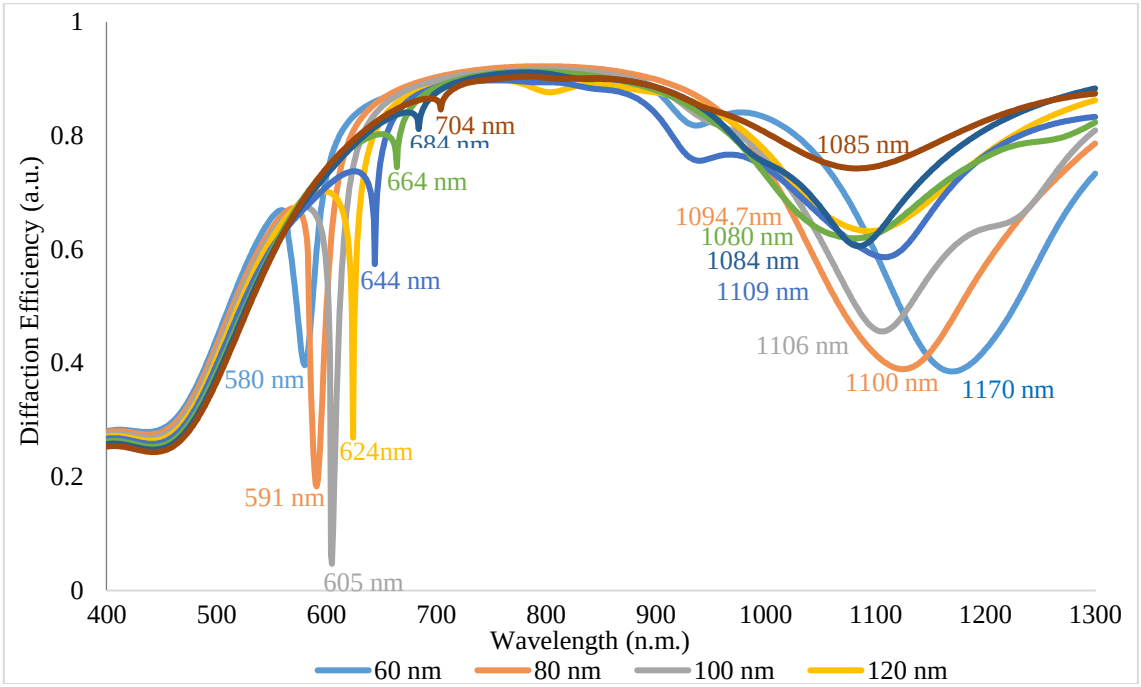

Figure 3.10 Diffraction efficiency VS wavelength curve in presence of target biomolecule

Above graphs show the reflection response in case of wide gap regime on altering the grating spacing, the resonance wavelengths have been tabulated in the following table for better understanding of the result.

Table 3.3 Comparison for shift in wavelengths for various grating interspacings.

Grating Interspacing (d) (nm)	**Without biomolecule (nm)**		**With biomolecule (nm)**		**Shift (nm)**	
	Dip 1	**Dip 2**	**Dip 1**	**Dip 2**	**1**	**2**
60	573	1143	580	1170	7	27
80	584	1100	591	1125	7	25
100	600	1090	605	1106	5	16
120	620	1081	624	1094.7	4	13.7
140	640	1066	644	1109	4	43
160	660	1075	664	1080	4	5
180	680	1065	684	1084	4	19
200	700	1070	704	1085	4	15

As can be seen from the above table, general response after target molecule capture is red shift in resonance wavelength. Although two resonance points are attained for all the cases but the results are not consistent in any manner when the grating gap is increased, that is it is difficult to predict the nature of response from previous results.

3.2.2 Effect of varying grating height (*h*)

In the previous section grating interspacing is altered and although results are a bit random, best results are attained in case of 60 nm grating gap, which hold quite true to observations from narrow regime gratings that smaller the grating gap, better is the result. Therefore here 60 nm grating gap is used. The grating width is kept constant at w = 500nm and grating heights are varied from 50 nm to 250 nm with 50 nm steps. The diffraction efficiency vs wavelength curve for above specifications is plotted which is as shown in fig. 3.11

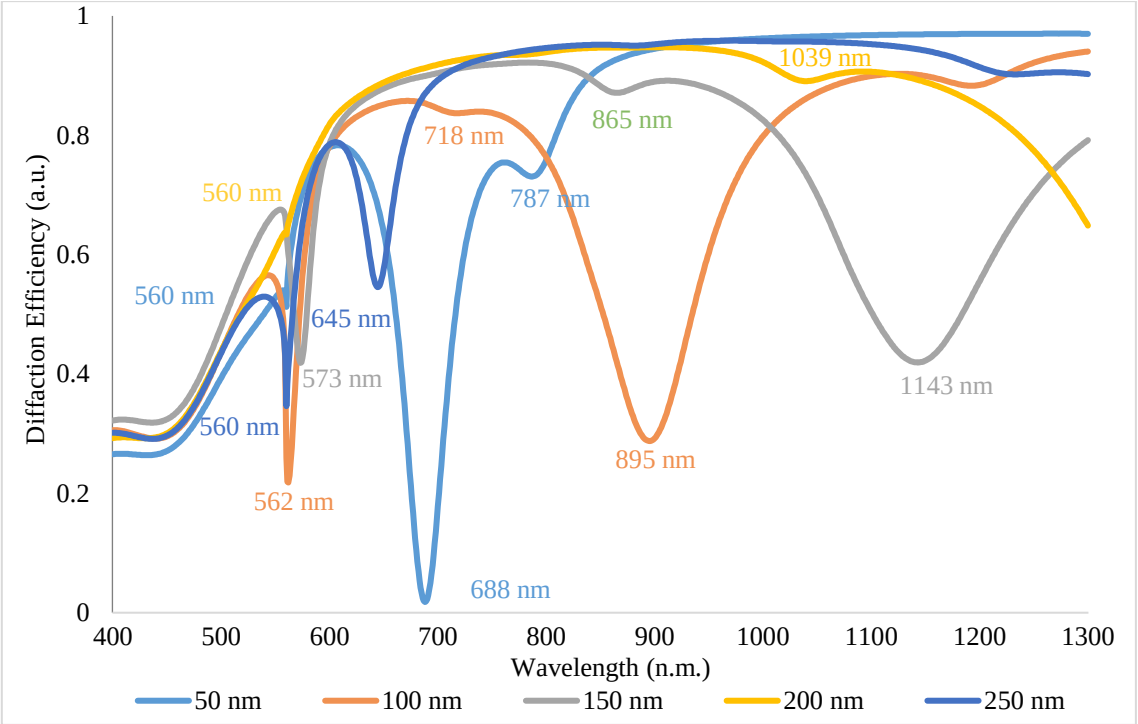

Figure 3.11 Diffraction efficiency VS wavelength curve with varying grating spacing

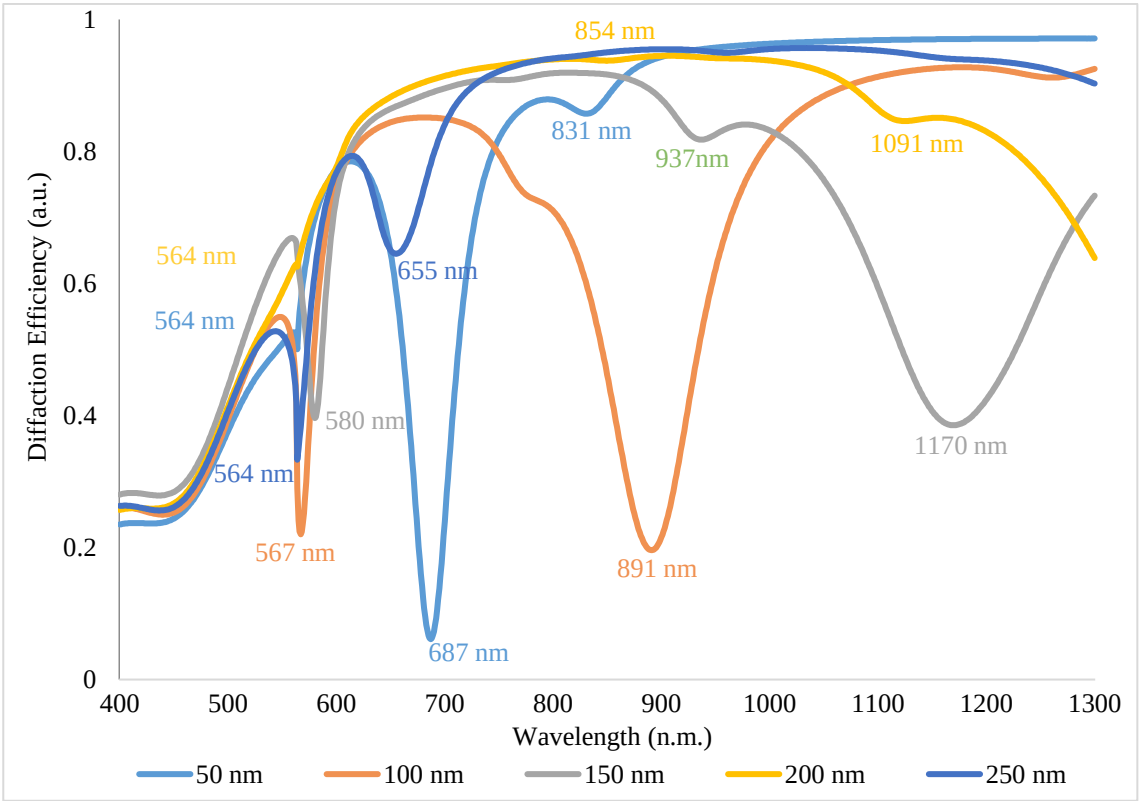

Figure 3.12 Diffraction efficiency VS wavelength curve in presence of target biomolecule

Above graphs show the reflection response in case of wide gap regime on altering the grating spacing, the resonance wavelengths have been tabulated in the following table for better understanding of the result.

Table 3.4 Comparison for shift in wavelengths for various grating interspacings.

Grating Height (nm)	Without biomolecule (nm)			With biomolecule (nm)			Shift (nm)		
	Dip 1	**Dip 2**	**Dip 3**	**Dip 1**	**Dip 2**	**Dip 3**	**1**	**2**	**3**
50	560	688	787	564	687	831	4	-1	44
100	562	718	895	567	null	891	5	null	-4
150	573	865	1143	580	937	1170	7	72	27
200	560	718	1039	564	854	1091	4	136	52
250	560	645	null	564	655	null	4	10	null

As can be seen from the above table, general response after target molecule capture is red shift in resonance wavelength. It is observed, as the grating height is increased, newer modes are introduced and the separation between modes is also increased.

3.3 CONCLUSIONS

We have modelled and simulated various nanostructures in section 3.1 and 3.2. From the readings in the previous sections, following can be concluded:

- In case of uniform grating heights, for narrow gap regime, best results are observed at 2 nm gap.
- In case when the inter-grating gap is kept constant and grating height is varied, multiple peaks and better sensitivity are obtained for narrow gap regime at 250 nm height

As has been mentioned in section 3.1, the regime of interest is the narrow gap regime, therefore a nanograting sensor with optimised specifications for narrow gap regime has been modelled and the resulting diffraction VS wavelength curve is as given in fig. 3.13. Fig. 3.13 shows two curves representing the sensor before target molecule is captured and the other representing in presence of the target biomolecule, followed by fig. 3.14 showing the electric field distribution around the sensor.

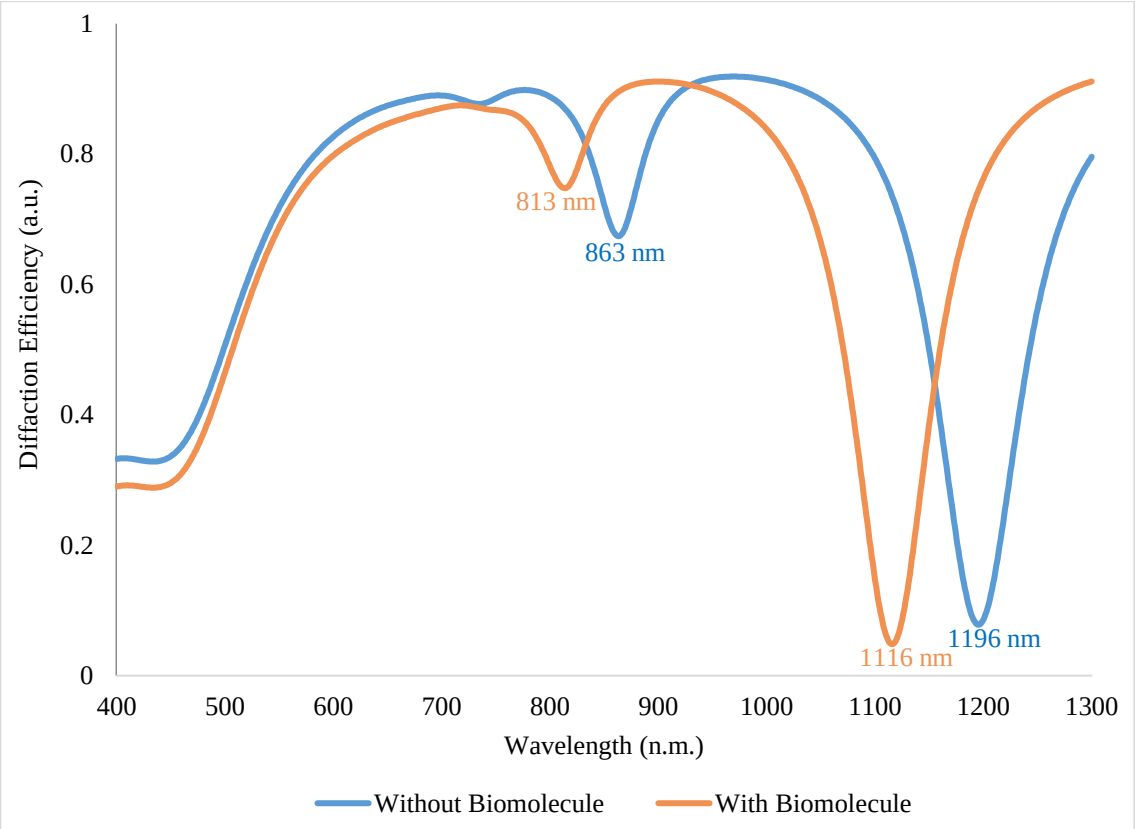

Figure 3.13 Comparison curves for the optimised sensor

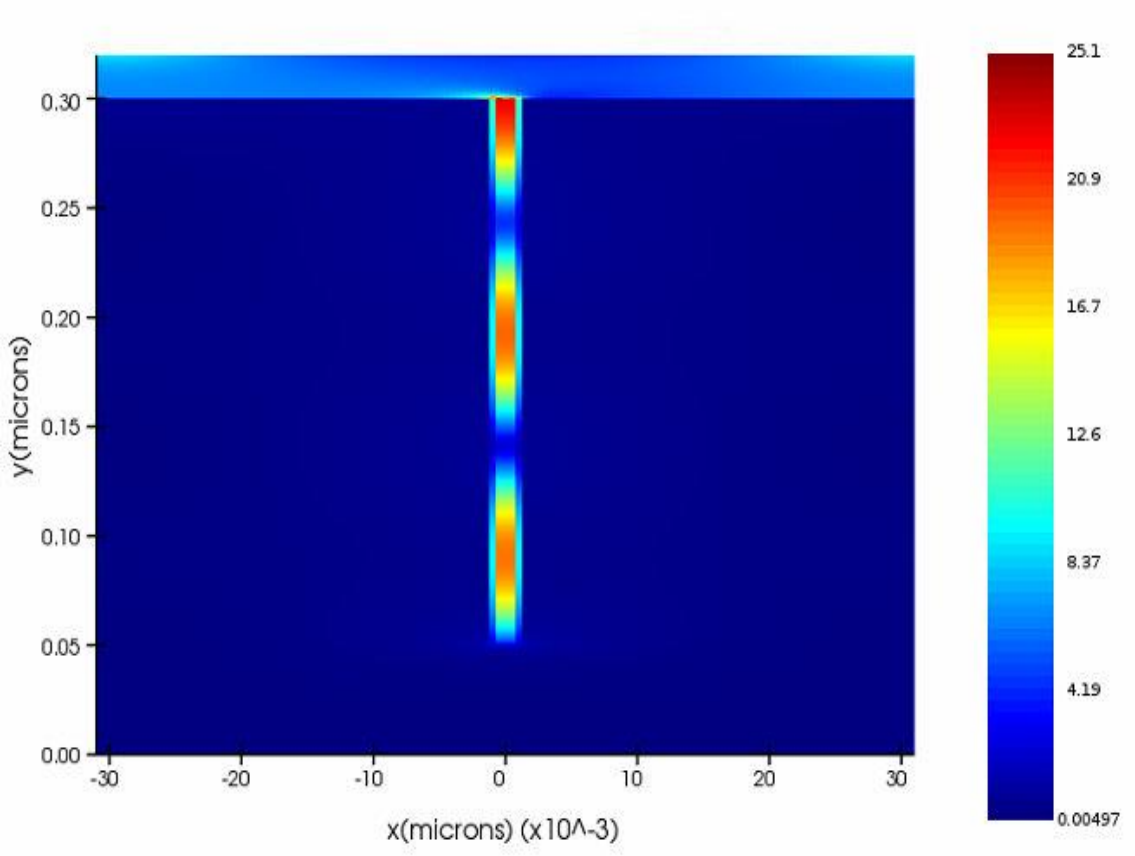

Figure 3.14 E-Field distribution for a sensor in case of target detection

CHAPTER 4

PLASMONIC MODES IN AN ASYMMETRIC NANOGRATING

In the previous chapter, the changes caused in the resonance wavelength due to change in a geometrical parameter were observed, i.e., the grating interspacing or the grating height. Further, all our previous studies corresponded to symmetric designs, that is, all the individual gratings are kept at uniform distance to each other and all of them have equal heights as is given in fig. 4.1(a). It is interesting to analyse the response of the sensor when parameters from different symmetric structures are integrated to make a single sensor. This section address whether there would be a unique response and where the previous resonance peaks are assimilated. An example of such sensor design is shown in fig. 4.1(b).

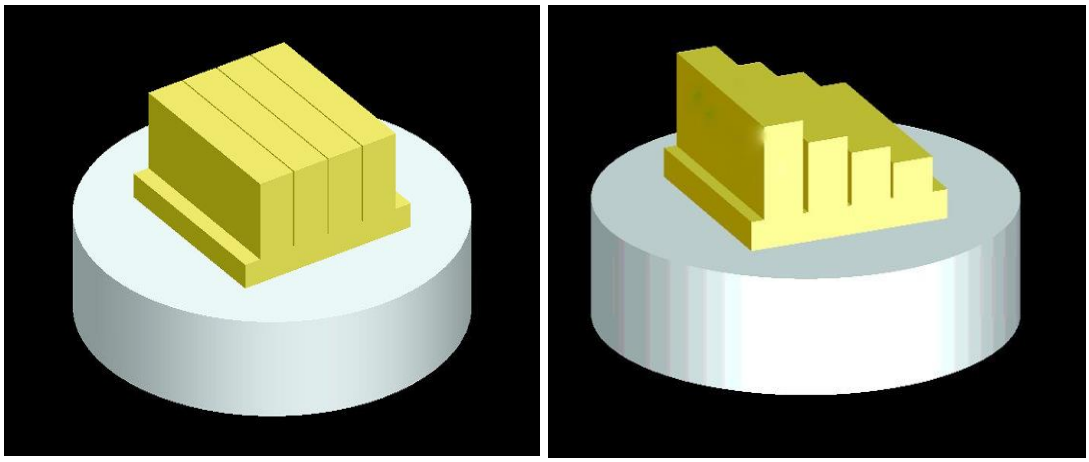

Figure 4.1 (a) Symmetric grating sensor **(b)** Asymmetric grating structure

The above questions can be answered by designing a sensor which has asymmetric parameters in a unit period. Therefore, in this chapter a sensor which has grating heights in a periodic rotation of 80 nm, 60 nm and 40 nm has been modelled. Along with the asymmetric heights, asymmetric grating interspacings have been analysed by setting the grating spacing to 8 nm, 6 nm and 4 nm respectively. The sensor design is shown in fig. 4.2. The gratings are made over a 50 nm thin gold film.

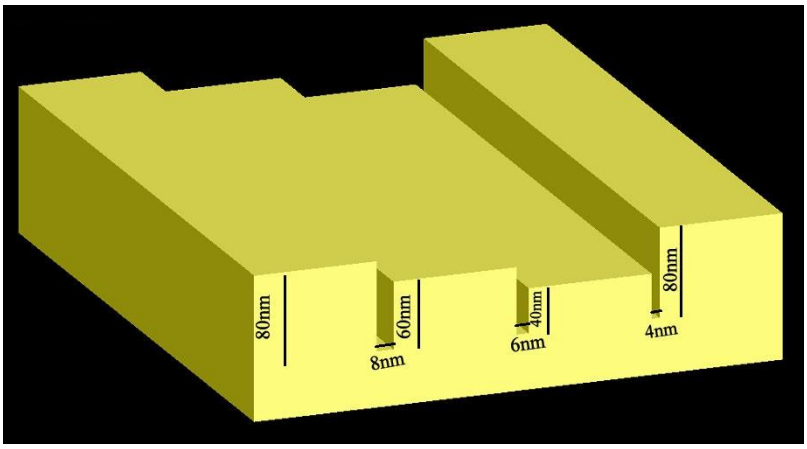

Figure 4.2 Specifications for the sensor structure under consideration

The numerical solution for above mentioned sensor, solved using rigorous coupled wave analysis (RCWA) method resulted in diffraction efficiency vs wavelength curve as following:

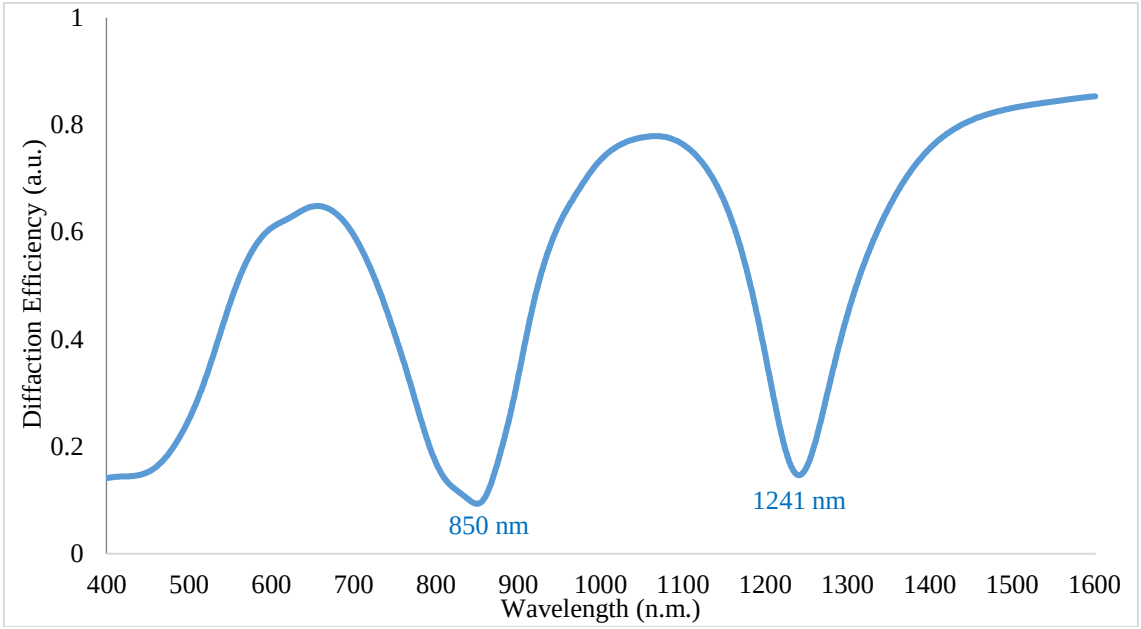

Figure 4.3 Response of sensor through the spectrum

As can be seen from fig. 4.3, there are two points of resonance at 850 nm and 1241 nm respectively. The asymmetric grating structure that has been used for this study can be said to be composed of parts of symmetric gratings, each of which has 80nm or 60nmor 40 nm individually and also a grating interspacing of 8nm or 6nm or 4 nm. The following section shows the individual curves that sum up together to form the two resonances.

The following fig. 4.4 shows us the diffraction efficiency vs wavelength curve for the structures involved for the first resonance wavelength at 850nm.

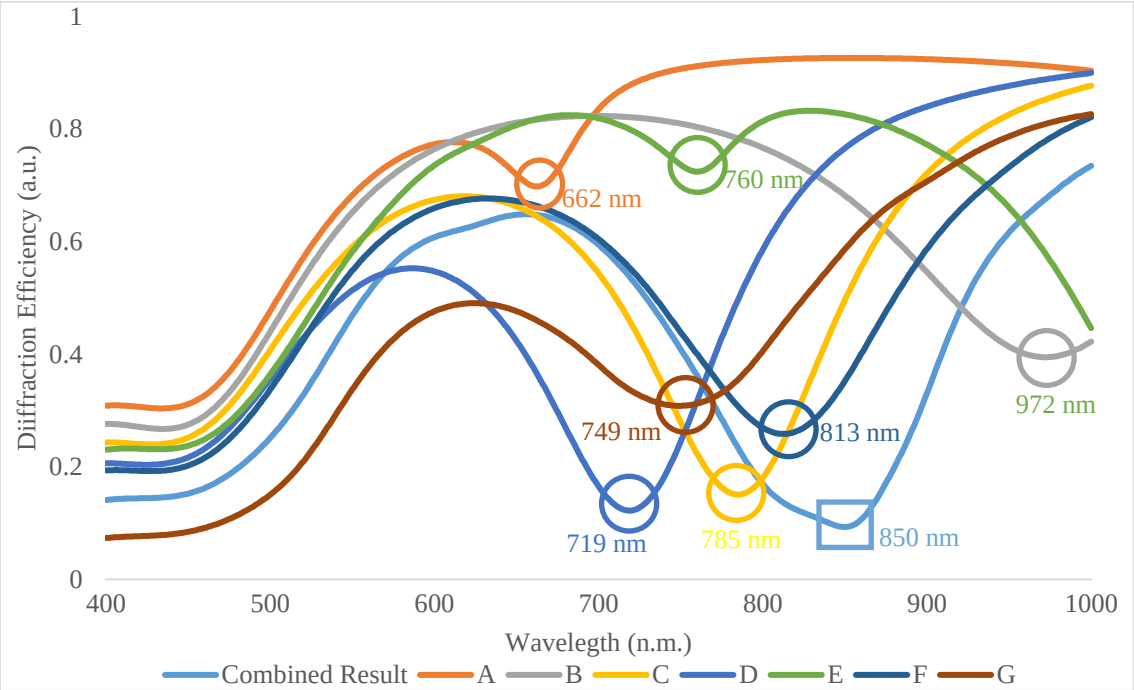

Figure 4.4 Combined response

The following table tells us about the individual structure that contributes to resulting resonance:

Table 4.1 Resonance wavelength of structures contributing to the first dip in asymmetric structure.

	Height 1 (nm)	**Spacing 1 (nm)**	**Height 2 (nm)**	**Spacing 2 (nm)**	**Height 3 (nm)**	**Spacing 3 (nm)**	**Resonant Wavelength (nm)**
A	80	4	Periodic				662
B	60	6	Periodic				972
C	40	6	Periodic				785
D	40	8	Periodic				719
E	80	4	60	4	Periodic		760
F	60	6	40	6	Periodic		813
G	80	8	40	8	Periodic		749

An observation can be made from above table that most contributing structures show a red shift in nature with structure b alone showing a blue shit in resonance. As is observed from above graph and table specification a, c, d, e, f, g result in a red shift of curve. A similar observation can be made for second wavelength dip, for which the resonance wavelengths are shown in fig. 4.5

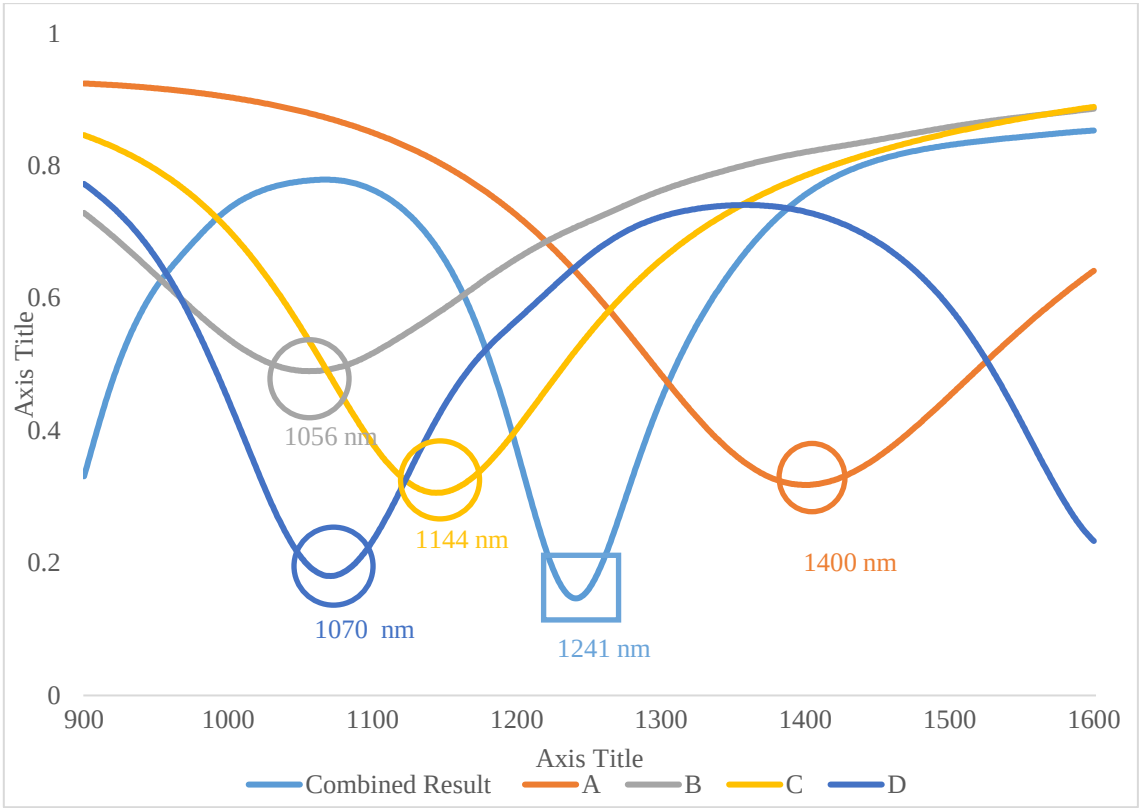

Figure 4.5 Combined response

The following table tells us about the individual structure that contributes to resulting resonance:

Table 4.2 Resonance wavelength of structures contributing to the second dip in asymmetric structure.

	Height 1 (nm)	**Spacing 1 (nm)**	**Height 2 (nm)**	**Spacing 2 (nm)**	**Height 3 (nm)**	**Spacing 3 (nm)**	**Resonant Wavelength (nm)**
A	80	4	Periodic				1400
B	80	8	Periodic				1056
C	60	4	Periodic				1144
D	80	4	60	4	80	4	1070

Similar observations to previous section can be made from above table that most contributing structures show a red shift in nature with structure b alone showing a blue shit in resonance. As is observed from above graph and table specification b, c, d result in a red shift of curve.

The main point of observation is the amount of Reflection shown at the resonance points. This reflectance is clearly much less than the contributing structures. A dip in the reflectance curve represents that field enhancements at those points are particularly high which lead to a better sensitivity.

CHAPTER 5

ASYMMETRIC NANO-GRATINGS AS PLASMONIC SENSORS

The preceding chapter helps us understand the fact that hybridising parameters from various symmetric gratings raises the possibility of a designing a sensor structure with better sensitivity and multiple resonance wavelengths. It is an established fact that behavioural properties of a sensor can be altered by varying its physical dimensions. Our objective is to design a sensor with improved sensitivity and increased wavelengths of applicability. We strive to achieve so by improving on our previous designs. In chapter 3, we altered parameters of a symmetric grating and observed their response to determine various factors for the optimised sensor design. We improve on that approach by using an asymmetric gratings design. In this chapter we study a structure similar to fig. 5.1.

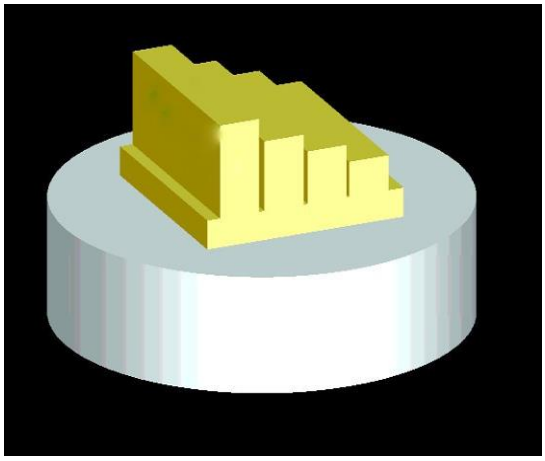

Figure 5.1 Asymmetric grating design

In the fig. 5.1, we see a single unit of structure which is periodically repeated in order to achieve our grating sensor design. We shall study this structure design in three sections:

- Three differing grating heights in a unit.
- Four differing grating heights in a unit.
- Four differing grating gaps in a unit.

In chapter 3 we had reached the conclusion that smaller inter-grating spacing leads to better results. Also, we achieved best readings for 2 nm inter-grating spacing. Therefore, for section 5.1 and section 5.2, we use 2 nm grating gap as a standard. After an

optimum grating height ratio is decided from section 5.1 and section 5.2, we will then study the effect of variation of inter-grating spacing. In this section, instead of having constant inter-grating spacing, we alter the gaps in a manner such that they are in some defined ratio. For all the mentioned scenarios, we shall study the sensor response for both the cases when only sensor is present as well as in the presence of biomolecule. Refractive index for the biomolecule is taken to be 1.58 and the gold nanogratings are imposed over a 50 nm thin gold film.

5.1 VARYING GRATING HEIGHTS

In a plasmonic sensor, the resonance wavelength is highly dependent on the physical structure of sensor, as has also been seen from the previous studies. In this section, work towards a heterogeneous or asymmetric design is discussed in which the grating heights are varied, for better modelling results, the work is further subdivided to two sections

5.1.1 Three gratings in a unit

Sensor designs with a periodicity of three grating heights are discussed in this section. The gratings have a width of 60 nm and are arranged with grating spacing of 2 nm, the reason being improved E field enhancements and increased number of resonance wavelengths for smaller grating spacing. The mentioned reasoning has been verified via results from previous sections. The gratings are built over a 50 nm thin gold film. The grating heights are taken to be in integral ratio to each other in order to achieve consistency in results. The considered ratios are (a) 3:2:1 (b) 4:3:2 (c) 5:4:3 (d) 5:3:1. Resulting diffraction efficiency vs wavelength for each variation has been plotted and are as follows:

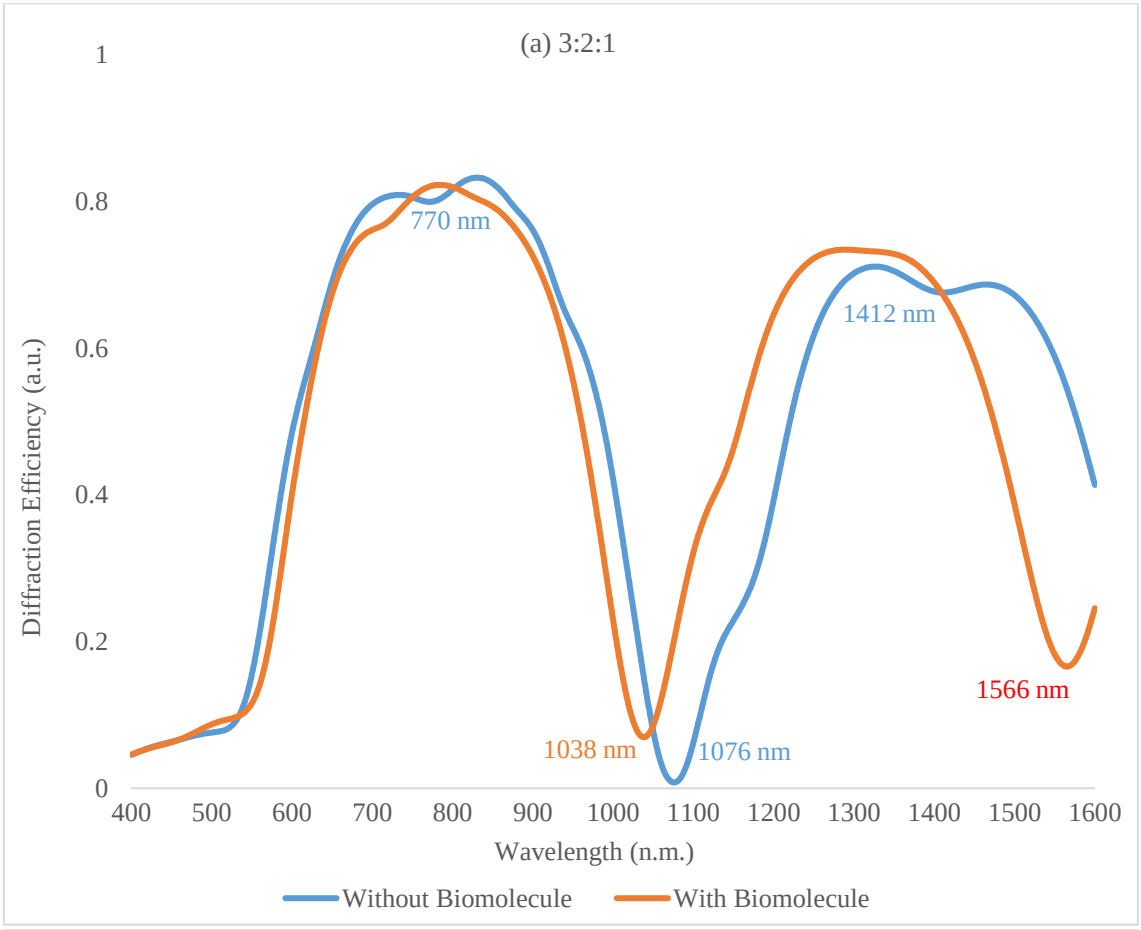
(a) 3:2:1
Diffraction Efficiency (a.u.)
1
0.8
0.6
0.4
0.2
0
770 nm
1412 nm
1566 nm
1038 nm
1076 nm
400 500 600 700 800 900 1000 1100 1200 1300 1400 1500 1600
Wavelength (n.m.)
Without Biomolecule
With Biomolecule

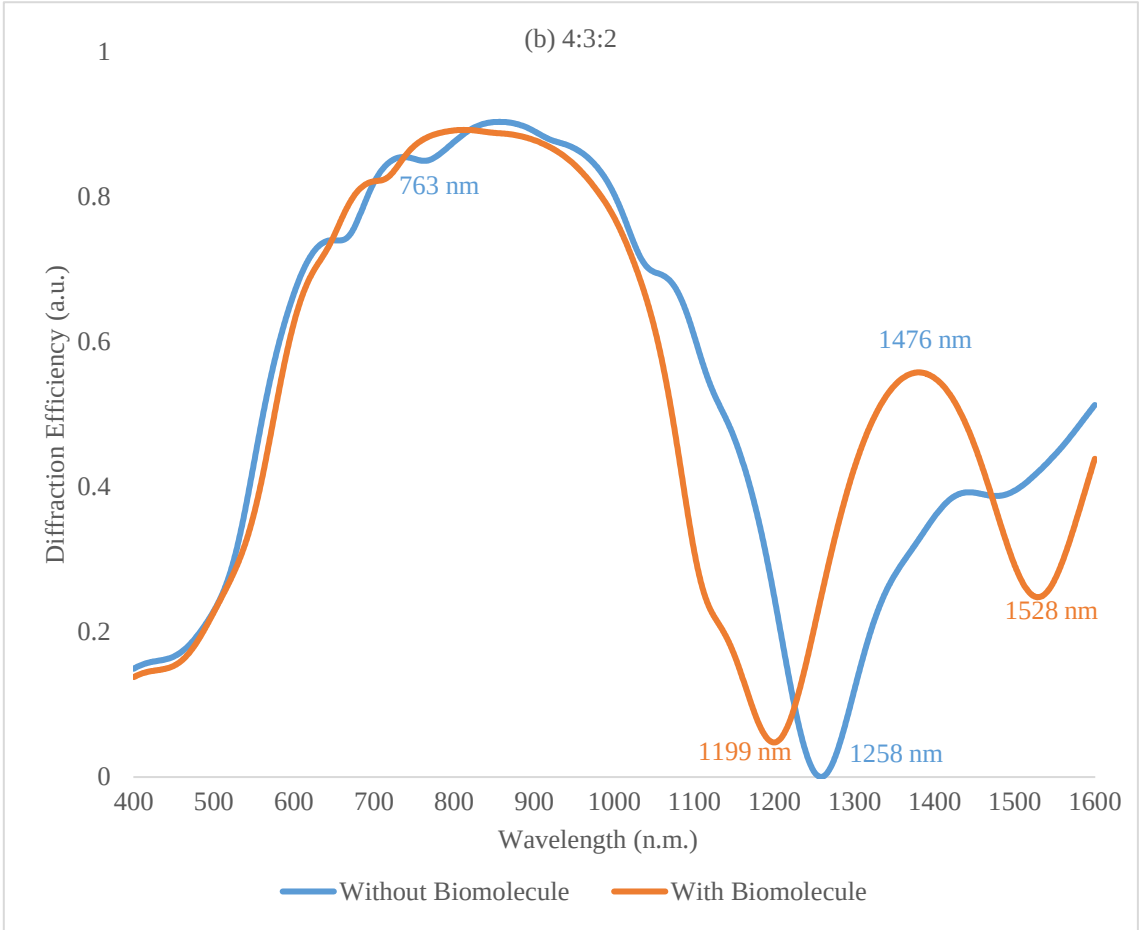
(b) 4:3:2
Diffraction Efficiency (a.u.)
1
0.8
0.6
0.4
0.2
0
763 nm
1476 nm
1528 nm
1199 nm
1258 nm
400 500 600 700 800 900 1000 1100 1200 1300 1400 1500 1600
Wavelength (n.m.)
Without Biomolecule
With Biomolecule

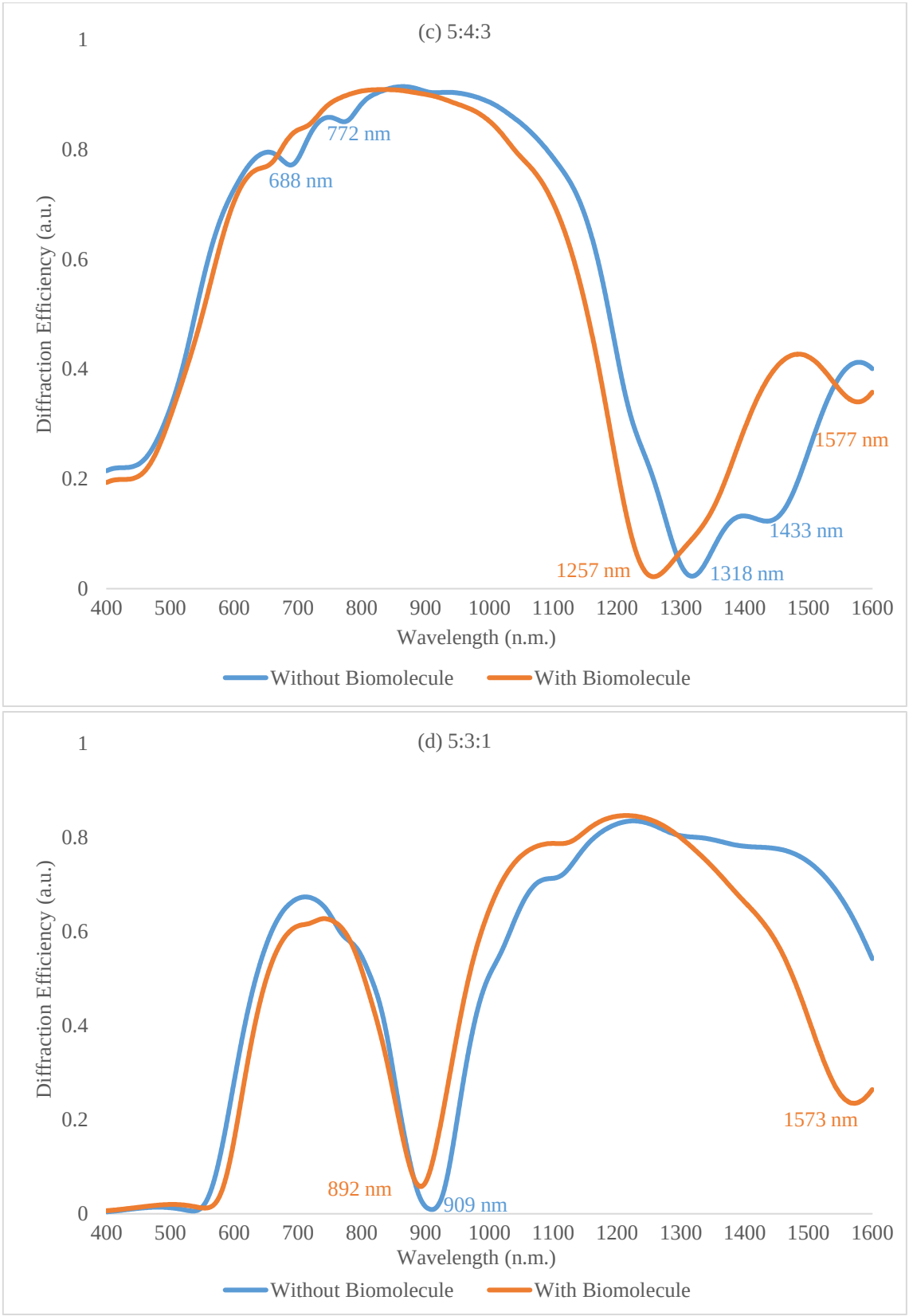

Figure 5.2 Diffraction Efficiency VS wavelength curve for grating heights in varying ratios **(a)** 3:2:1 **(b)** 4:3:2 **(c)** 5:4:3 **(d)** 5:3:1

As is seen from the graphs, most results give blue shift at resonance wavelength. The wavelength dips have been tabulated and although lower reflectance is

observed at resonance wavelengths implying high E filed enhancements, the number of resonance wavelengths obtained has been decreased in comparison to the optimised symmetric sensor from section 3.

Table 5.1 Comparison for shift in wavelengths for various grating height ratio.

Height Ratio	Without biomolecule (nm)			With biomolecule (nm)			Shift (nm)		
	Dip 1	Dip 2	Dip 3	Dip 1	Dip 2	Dip 3	1	2	3
3:2:1	770	1076	1412	null	1038	1566	null	-38	154
4:3:2	null	1258	1476	null	1199	1528	null	-59	52
5:4:3	null	1318	null	null	1257	1577	null	-61	null
5:3:1	909	null	null	892	null	1572	-17	null	null

From above observations, any significant improvement over proposed optimised sensor design from section 3 are not attained. This result might be attributed to some of the grating heights to be small resulting in low *h:d* ratio.

5.1.2 Four gratings in a unit

A broader variation to grating heights is introduced in order to improve upon results from section 5.1.1 by including an additional grating height ratio. The gratings heights are in integral ratios and are imposed over a 50 nm thin gold film. The grating width is taken to be 60 nm with 2 nm grating gap between them. Biomolecule layer for target capture simulations is taken to be of 2 nm thickness with refractive index of 1.58. Modelled grating height ratios are (a) 4:3:2:1 (b) 5:4:3:2 (c) 6:5:4:3 (d) 7:6:5:4 (e) 7:5:3:1 and (f) 10:7:4:1. Resulting diffraction efficiency vs wavelength for each sensor design has been plotted and are as follows:

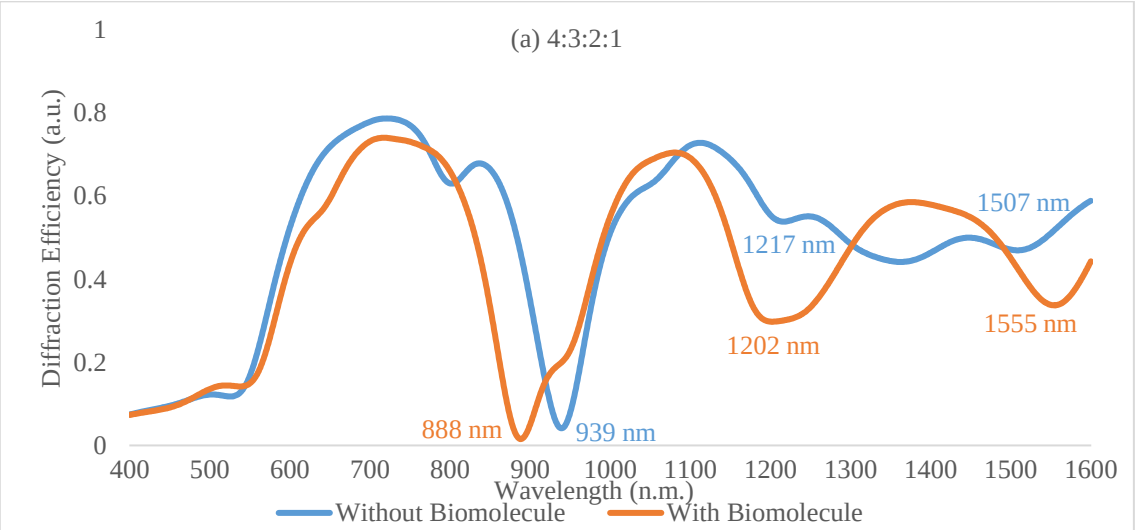

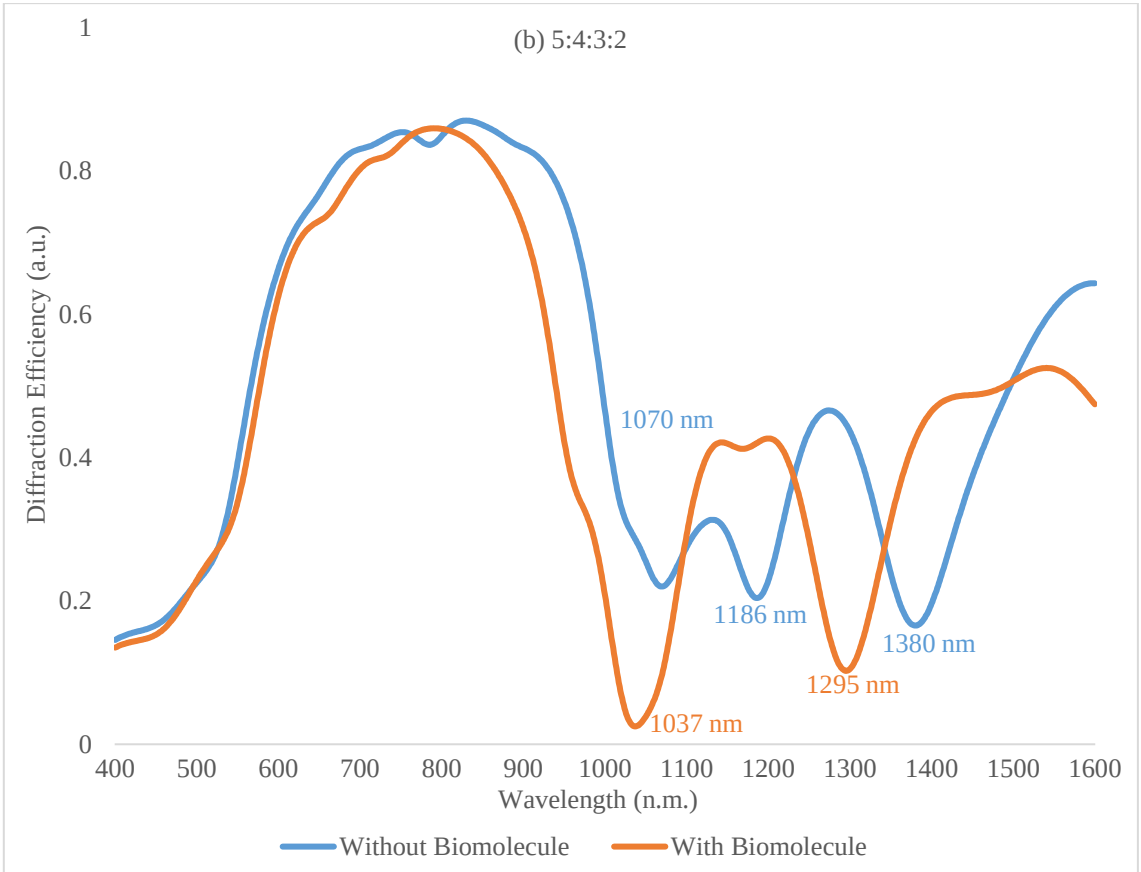
(b) 5:4:3:2
Diffraction Efficiency (a.u.)
1
0.8
0.6
0.4
0.2
0
400 500 600 700 800 900 1000 1100 1200 1300 1400 1500 1600
Wavelength (n.m.)
1070 nm
1186 nm
1380 nm
1295 nm
1037 nm
Without Biomolecule
With Biomolecule

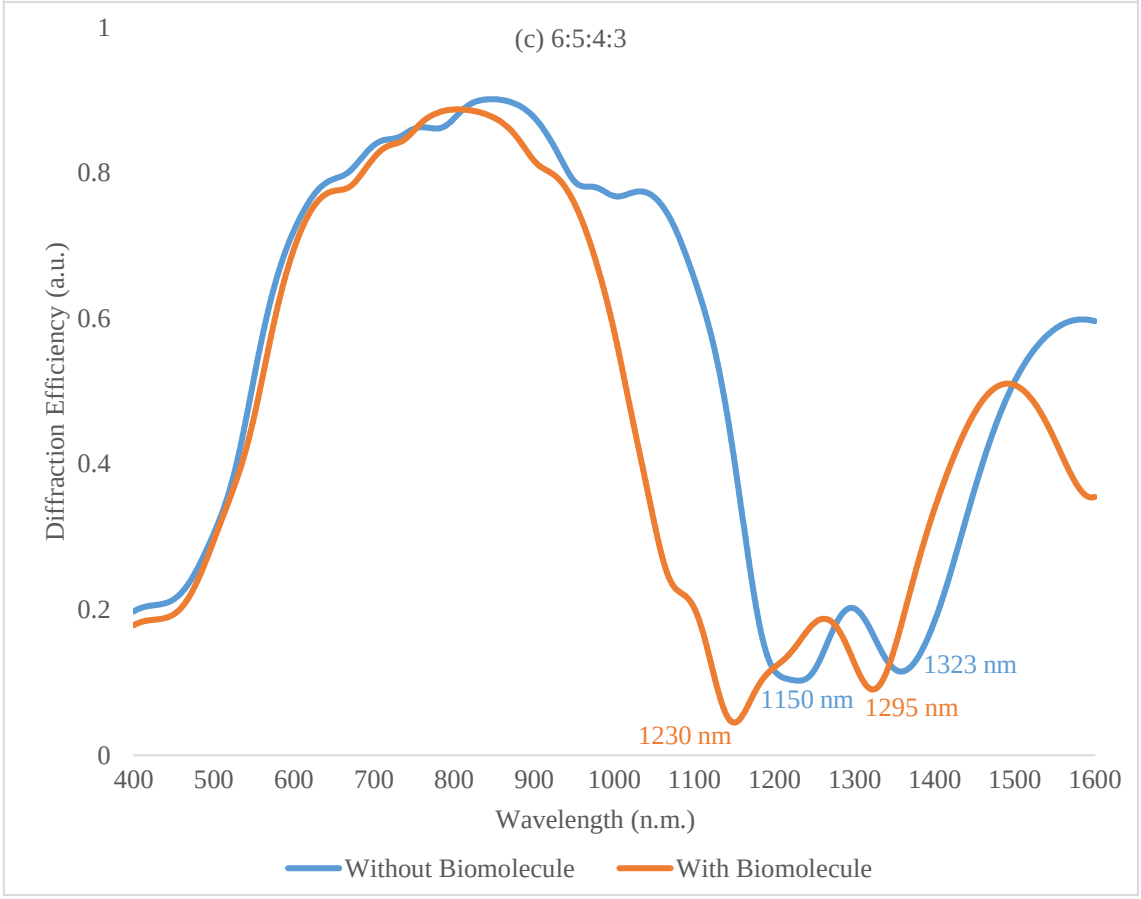
(c) 6:5:4:3
Diffraction Efficiency (a.u.)
1
0.8
0.6
0.4
0.2
0
400 500 600 700 800 900 1000 1100 1200 1300 1400 1500 1600
Wavelength (n.m.)
1323 nm
1150 nm
1295 nm
1230 nm
Without Biomolecule
With Biomolecule

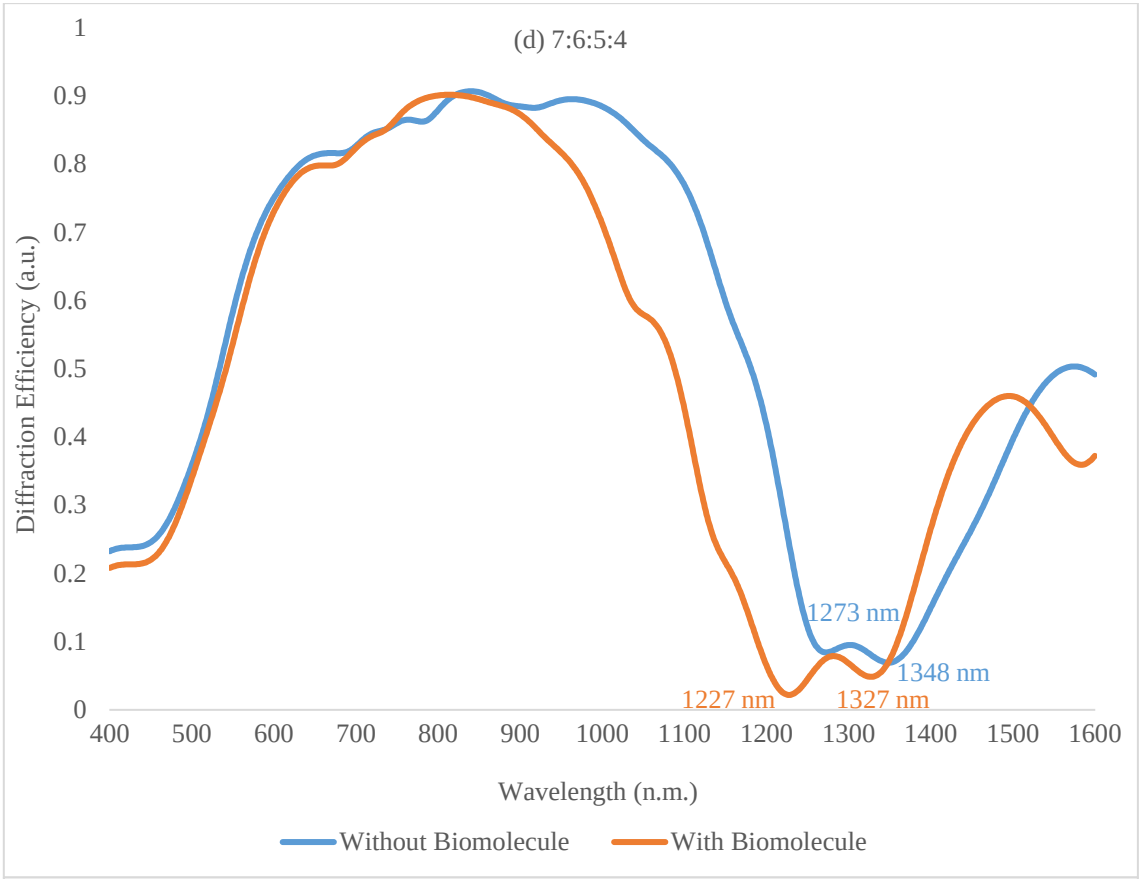
(d) 7:6:5:4
Diffraction Efficiency (a.u.)
1
0.9
0.8
0.7
0.6
0.5
0.4
0.3
0.2
0.1
0
400 500 600 700 800 900 1000 1100 1200 1300 1400 1500 1600
Wavelength (n.m.)
1273 nm
1348 nm
1227 nm
1327 nm
Without Biomolecule
With Biomolecule

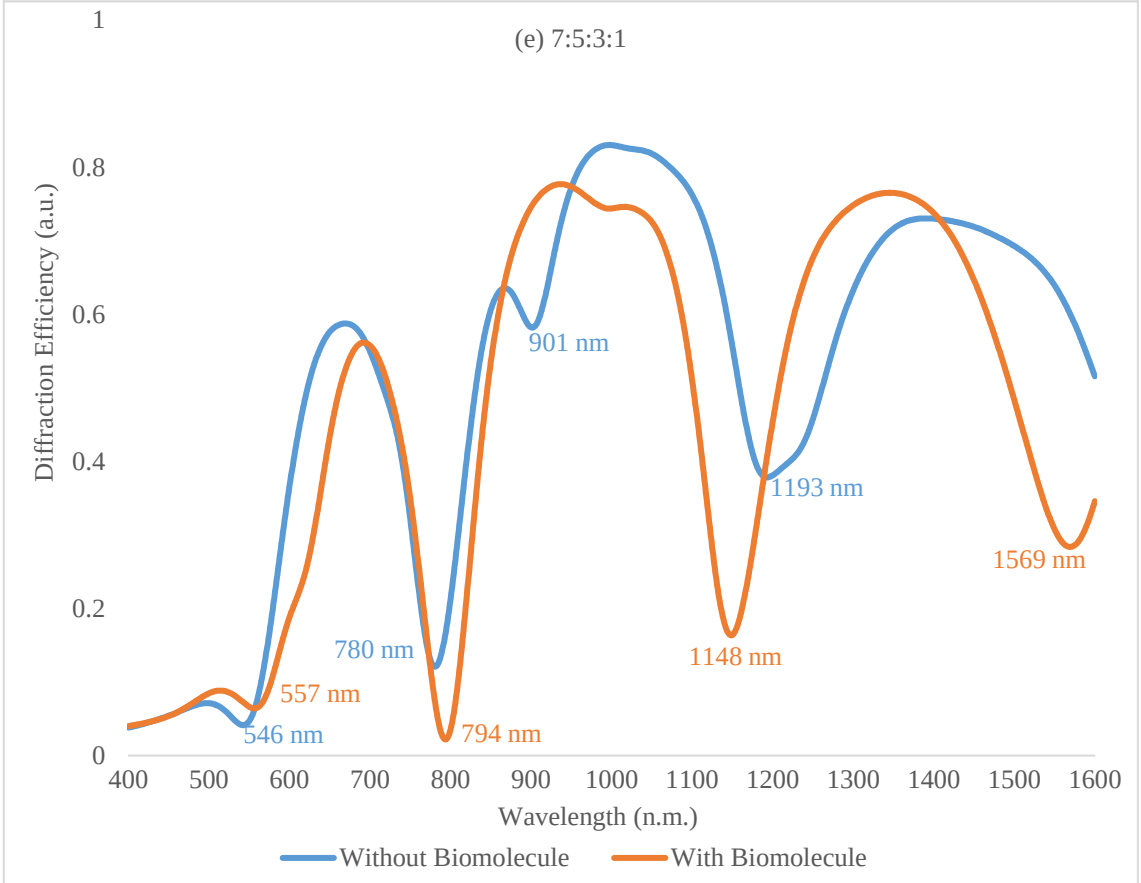
(e) 7:5:3:1
Diffraction Efficiency (a.u.)
1
0.8
0.6
0.4
0.2
0
400 500 600 700 800 900 1000 1100 1200 1300 1400 1500 1600
Wavelength (n.m.)
901 nm
1193 nm
1569 nm
780 nm
557 nm
546 nm
1148 nm
794 nm
Without Biomolecule
With Biomolecule

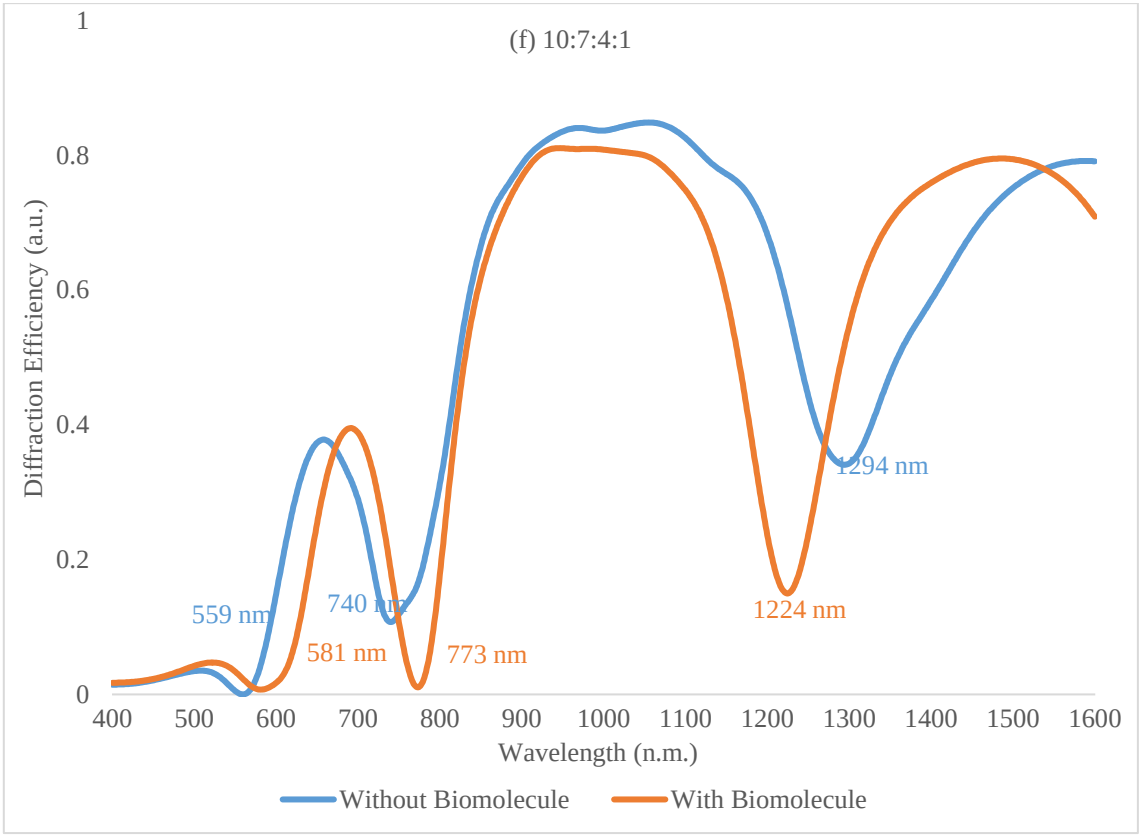

Figure 5.3 Diffraction Efficiency VS wavelength curve for grating heights in varying ratios **(a)** 4:3:2:1 **(b)** 5:4:3:2 **(c)** 6:5:4:3 **(d)** 7:6:5:4 **(e)** 7:5:3:1 **(f)** 10:7:4:1

As is seen from above graphs, most design results show three resonance wavelengths. In comparison to previous section, where at most, only 2 resonance wavelengths were attained, this is a direct increase by 50%. The resonance wavelengths along with the shift observed for a particular ratio are as follows:

Table 5.2 Comparison for shift in wavelengths for various grating height ratio.

Height Ratio	**Without biomolecule (nm)**			**With biomolecule (nm)**			**Shift (nm)**		
	Dip 1	**Dip 2**	**Dip 3**	**Dip 1**	**Dip 2**	**Dip 3**	**1**	**2**	**3**
4:3:2:1	939	1217	1509	888	1202	1555	-51	-15	46
5:4:3:2	1070	1186	1380	null	1037	1295	null	-149	-85
6:5:4:3	null	1230	1358	null	1150	1323	null	-80	-35
7:6:5:4	null	1273	1348	null	1227	1327	null	-46	-21
7:5:3:1	546	780	1193	557	794	1148	11	14	-45
10:7:4:1	559	740	1294	581	773	1224	22	33	-70

As can be observed from above table, half the sensor designs show three resonance wavelength shifts. Among all the results, blue shift in resonance wavelength is observed in most cases. The case (f) shows three resonance wavelength shifts and also has

overall higher wavelength shift for individual cases. Therefore in further studies 10:7:4:1 is the grating height ratio that is considered to be optimised design over others.

5.2 FOUR WIDTHS RATIO

In order to design an optimised sensor, it is necessary that all the defining parameters are at optimised values. In the previous section, 10:7:4:1 ratio grating height were attained as the optimised grating height ratios. In this section, the grating interspacing are taken to be in integral ratios to each other. The gratings are designed over 50 nm thin gold film and the grating width is taken to be 60 nm wide. Since the design under consideration is asymmetric in grating heights, the study for grating interspacing ratio is subdivided into following two sections:

5.2.1 Incremental order

The asymmetric gratings are called so for the lack of symmetry in the designed structure. Therefore, E field interaction is different if the same ratio of grating interspacing is applied in different order. In this section, the grating spacing are in an incremental ratio. The spacing ratios under consideration are (a) 1:2:3:4 (b) 2:3:4:5 (c) 3:4:5:6 (d) 4:5:6:7. The designed sensor is studied for both the cases capture mode and when the target molecule is detected and resulting diffraction efficiency VS wavelength graphs are drawn.

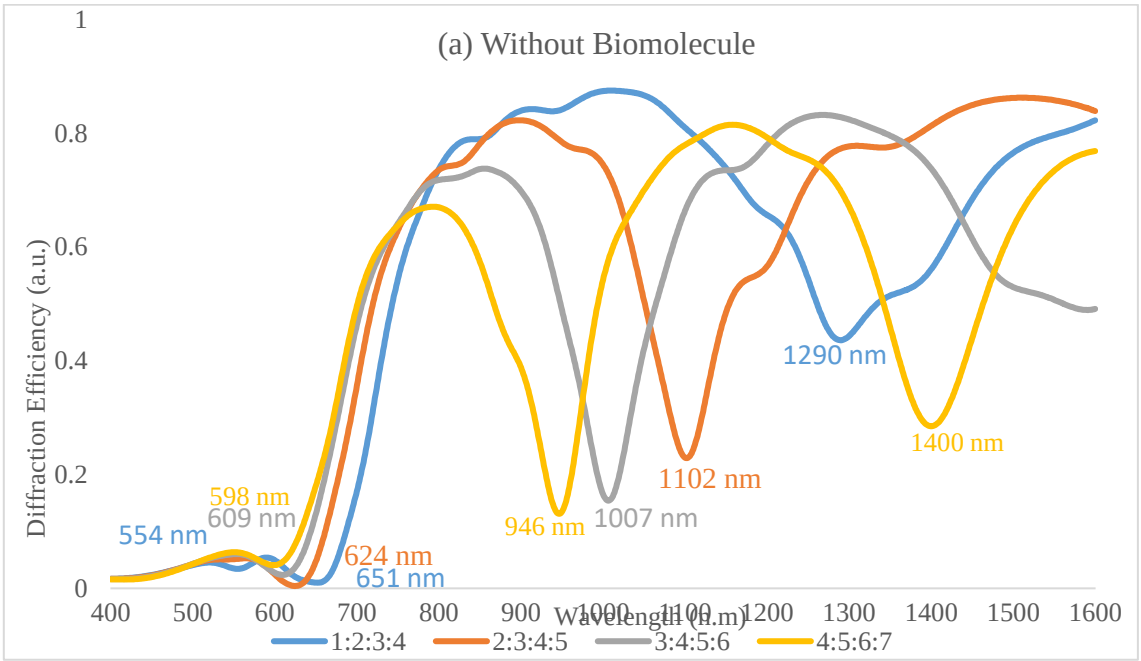

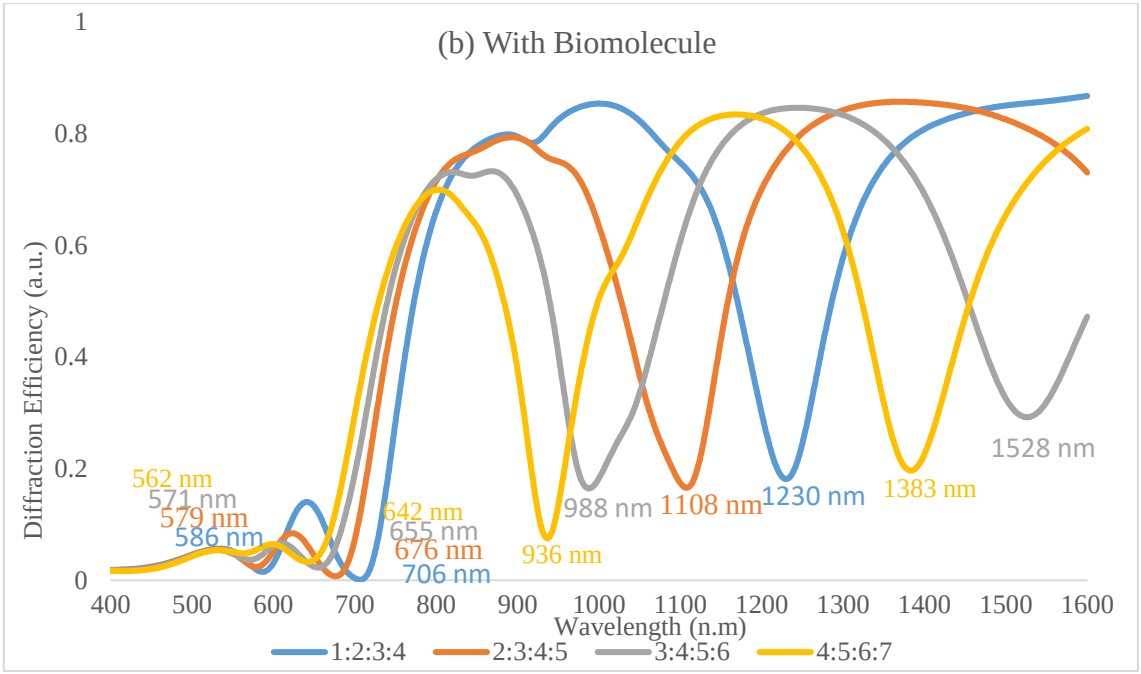

Figure 5.4 Diffraction Efficiency VS wavelength curve for grating heights in incremental ratio

Resulting resonance dips have been tabulated in table 5.3. It is observed that most resonance dips have a red shift. The best result is attained for ratio 1:2:3:4. Although the result is best among the presented grating ratio, it is still lacking in comparison to when the grating gap is kept constant at 2nm.

Table 5.3 Comparing resonance wavelengths for grating widths in incremental ratio

Height Ratio	Without biomolecule (nm)			With biomolecule (nm)			Shift (nm)		
	Dip 1	Dip 2	Dip 3	Dip 1	Dip 2	Dip 3	1	2	3
1:2:3:4	554	651	1290	586	706	1230	32	55	-60
2:3:4:5	null	624	1102	579	676	1108	null	52	6
3:4:5:6	null	609	1007	571	655	988	null	46	-19
4:5:6:7	null	598	946	562	642	null	null	44	null

5.2.2 Decremental Order

It has already been established that smaller d:h ratio leads to better plasmon resonance. Lack of improvement in comparison to results from section 3 in the previous section can be attributed to grating interspacing being considerably large in comparison to height of some of the grating pillars thus increasing *d:h* ratio. This is easily rectified by reversing the order of grating interspacing ratio. In this section, grating interspacing ratio are taken in decremental ratio, i.e. the ratio under consideration are (a) 4:3:2:1 (b) 5:4:3:2 (c)6:5:4:3 (d)7:6:5:4. Grating heights are in ratio of 10:7:4:1 and both cases for capture

mode and when the target molecule is detected are considered and resulting diffraction efficiency VS wavelength graphs are drawn.

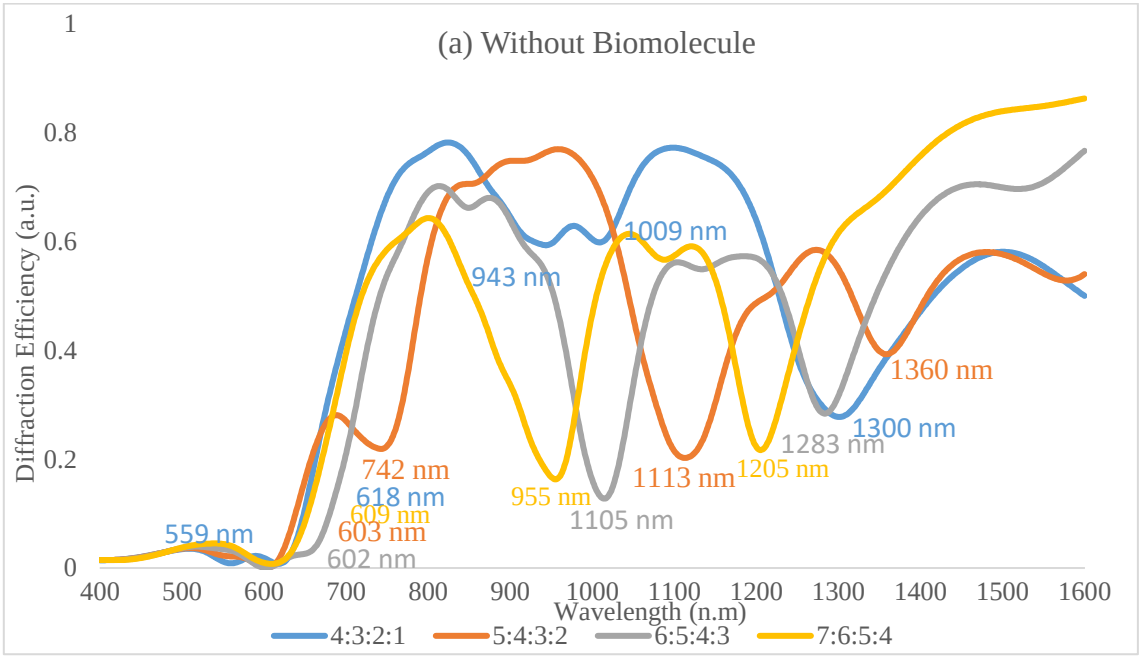

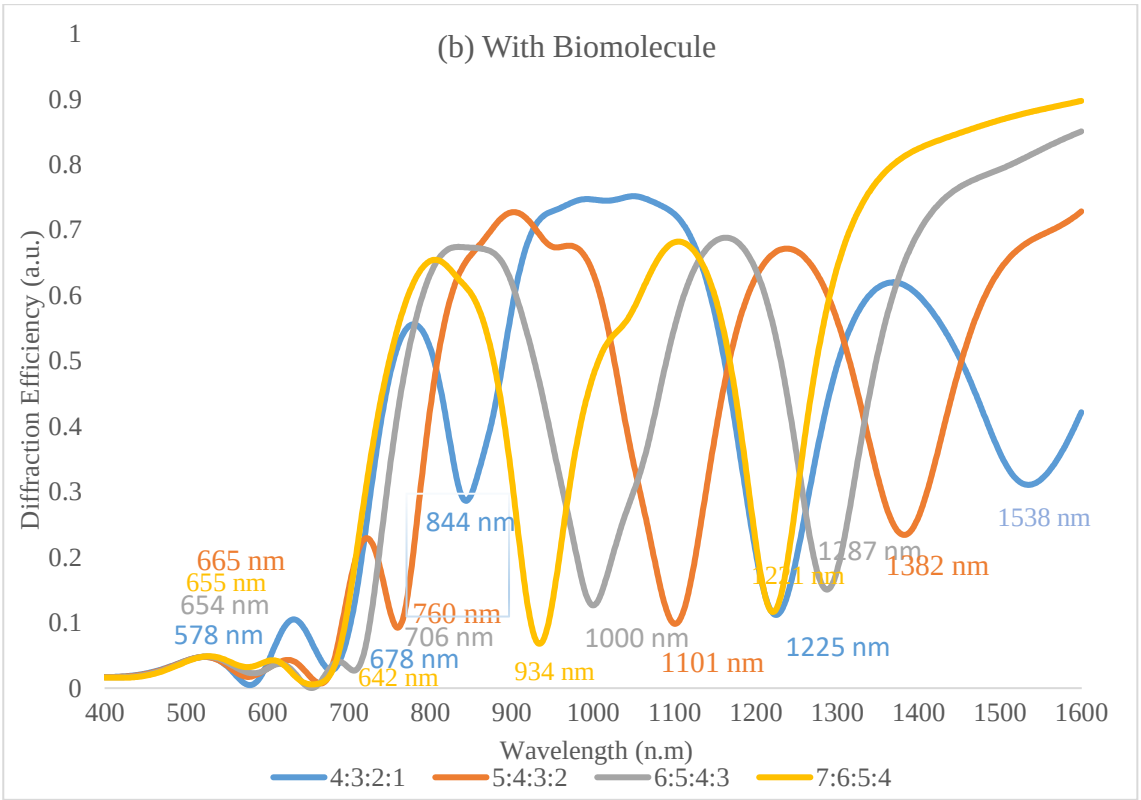

Figure 5.5 Diffraction Efficiency VS wavelength curve for grating heights in decremental ratio

As is seen from fig. 5.4 the number of resonance wavelength dips is considerably increased. Resonance wavelength dips data from above graphs is tabulated in the following table.

Table 5.4 Comparing resonance wavelengths for grating widths in decremental ratio

Grating Widths	**Without biomolecule (nm)**				**With biomolecule (nm)**				**Shift (nm)**			
	Dip 1	**Dip 2**	**Dip 3**	**Dip 4**	**Dip 1**	**Dip 2**	**Dip 3**	**Dip 4**	**1**	**2**	**3**	**4**
4:3:2:1	559	618	943	1300	578	678	844	1225	19	60	-99	-75
5:4:3:2	603	742	1113	1360	665	760	1101	1382	62	18	-12	22
6:5:4:3	602	null	1105	1283	654	null	1000	1287	52	null	-105	4
7:6:5:4	609	null	955	1205	655	null	934	1221	46	null	-21	16

From above the significant improvement in comparison to previous interspacing ratio is easily observed. The ratio 4:3:2:1 easily stands out to be the most optimal ratio in comparison to others as not only four resonance wavelength dip shifts occur but the wavelength shifts also have significant magnitude. This result easily outshines all the previous design and simulation results.

CHAPTER 6

CONCLUSIONS AND FUTURE WORK

The thesis begins with introduction to LSPR phenomenon which is elaborated upon in the following chapter. Chapter 2 also contains a brief review of research work done related to sensors built upon the surface plasmon resonance phenomena in the past few years. From literature reviews it is established that nanograting structures on a nano metal film provides significantly more sensitivity as compared to a thin nano metal film.

In chapter 3, symmetric nanogratings are designed and the diffraction efficiency VS wavelength curves are studied for both the case when the sensor is in capture mode and when in presence of target biomolecule. From the results the optimal asymmetric sensor dimensions turn out to be 2 nm grating interspacing and 250 nm grating height with grating width being 60 nm and the grating is imposed over a 50 nm thin gold film. The test target biomolecule is taken to have 1.58 refractive index which is similar to refractive index of DNA molecules. It is also concluded from the chapter that smaller values of *d:h* ratio leads to better field enhancements.

Chapter 4 leads the study towards asymmetric sensor structures and discusses the improvement in sensitivity results in a hybridised structure composed of various symmetric sensor structure parameters. Chapter 5 build upon previous results and the research is carried towards designing optimal asymmetric bio sensor. The design and simulation results from this chapter concludes to optimal asymmetric sensor having grating pillar heights in the ratio 10:7:4:1 and grating interspacing in the ratio 4:3:2:1. Grating pillar widths are 60 nm and the nanograting is imposed over a 50 nm thin gold film. Four resonance shifts are observed two of which show blue shift and the other showing red shifts the observed shifts are 19, 60, 99 and 75 in magnitude which is overall the best result obtained among all the sensor designs. As the asymmetricity in narrow-groove nanogratings, in the narrow gap regime, have proved to be highly sensitive to biomolecules, and large shifts in the resonance wavelength have been obtained with higher degrees of asymmetricity, the effect of introducing more degrees of asymmetry can be exhaustively

analysed. Furthermore, the fabrication of such nanogratings by employing 3-D lithographic tools with high resolution can be attempted. The fabrication of such gratings is a challenging procedure and can be explored by employing 3-D electron beam deposition, or hybrid methods.

REFERENCES

[1]. Van Duyne RP. 2004. Molecular plasmonics. *Science* 306:985–86

[2]. Haes, A. J., Haynes, C. L., McFarland, A. D., Schatz, G. C., Van Duyne, R. P., & Zou, S. (2005). Plasmonic materials for surface-enhanced sensing and spectroscopy. *MRS bulletin*, *30*(5), 368-375.

[3]. Kelly, K. L., Coronado, E., Zhao, L. L., & Schatz, G. C. (2003). The optical properties of metal nanoparticles: the influence of size, shape, and dielectric environment.

[4]. Grunin, A. A., Zhdanov, A. G., Ezhov, A. A., Ganshina, E. A., & Fedyanin, A. A. (2010). Surface-plasmon-induced enhancement of magneto-optical Kerr effect in all-nickel subwavelength nanogratings. *Applied Physics Letters*, *97*(26), 261908.

[5]. Bozhevolnyi, S. I., Erland, J., Leosson, K., Skovgaard, P. M., & Hvam, J. M. (2001). Waveguiding in surface plasmon polariton band gap structures. *Physical Review Letters*, *86*(14), 3008.

[6]. De, A., & Puri, A. (2003). Kerr-resonance-condition-coupled enhancement in magneto-optic media. *Journal of applied physics*, *93*(2), 1120-1126.

[7]. Khanikaev, A. B., Baryshev, A. V., Fedyanin, A. A., Granovsky, A. B., & Inoue, M. (2007). Anomalous Faraday effect of a system with extraordinary optical transmittance. *Optics Express*, *15*(11), 6612-6622.

[8]. Belotelov, V. I., Bykov, D. A., Doskolovich, L. L., Kalish, A. N., & Zvezdin, A. K. (2009). Extraordinary transmission and giant magneto-optical transverse Kerr effect in plasmonic nanostructured films. *JOSA B*, *26*(8), 1594-1598.

[9]. Jen, S. U., & Chen, K. C. (2005). Enhancement of polar Kerr effect by forming Au nanoparticles on Ni surface. *Journal of applied physics*, *97*(10), 10M311.

[10]. Tomita, S., Kato, T., Tsunashima, S., Iwata, S., Fujii, M., & Hayashi, S. (2006). Magneto-optical Kerr effects of yttrium-iron garnet thin films incorporating gold nanoparticles. *Physical review letters*, *96*(16), 167402.

[11]. Armelles, G., Cebollada, A., García-Martín, A., García-Martín, J. M., González, M. U., González-Díaz, J. B., ... & Torrado, J. F. (2009). Magnetoplasmonic nanostructures: systems supporting both plasmonic and magnetic properties. *Journal of Optics A: Pure and Applied Optics*, *11*(11), 114023.

[12]. Konishi, K., Sugimoto, T., Bai, B., Svirko, Y., & Kuwata-Gonokami, M. (2007). Effect of surface plasmon resonance on the optical activity of chiral metal nanogratings. *Optics Express*, *15*(15), 9575-9583.

[13]. Ebbesen, T. W., Lezec, H. J., Ghaemi, H. F., Thio, T., & Wolff, P. A. (1998). Extraordinary optical transmission through sub-wavelength hole arrays. *Nature*, *391*(6668), 667.

[14]. Linden, S., Kuhl, J., & Giessen, H. (2001). Controlling the interaction between light and gold nanoparticles: selective suppression of extinction. *Physical review letters*, *86*(20), 4688.

[15]. Maier, S. A., & Atwater, H. A. (2005). Plasmonics: Localization and guiding of electromagnetic energy in metal/dielectric structures. *Journal of applied physics*, *98*(1), 10.

[16]. Elliott, J., Smolyaninov, I. I., Zheludev, N. I., & Zayats, A. V. (2004). Polarization control of optical transmission of a periodic array of elliptical nanoholes in a metal film. *Optics letters*, *29*(12), 1414-1416.

[17]. Anceau, C., Brasselet, S., Zyss, J., & Gadenne, P. (2003). Local second-harmonic generation enhancement on gold nanostructures probed by two-photon microscopy. *Optics letters*, *28*(9), 713-715.

[18]. Kim, K., Kim, D. J., Moon, S., Kim, D., & Byun, K. M. (2009). Localized surface plasmon resonance detection of layered biointeractions on metallic subwavelength nanogratings. *Nanotechnology*, *20*(31), 315501.

[19]. Campbell, C. T., & Kim, G. (2007). SPR microscopy and its applications to high-throughput analyses of biomolecular binding events and their kinetics. *Biomaterials*, *28*(15), 2380-2392.

[20]. He, L., Musick, M. D., Nicewarner, S. R., Salinas, F. G., Benkovic, S. J., Natan, M. J., & Keating, C. D. (2000). Colloidal Au-enhanced surface plasmon resonance for ultrasensitive detection of DNA hybridization. *Journal of the American Chemical Society*, *122*(38), 9071-9077.

[21]. Sepúlveda, B., Calle, A., Lechuga, L. M., & Armelles, G. (2006). Highly sensitive detection of biomolecules with the magneto-optic surface-plasmon-resonance sensor. *Optics letters*, *31*(8), 1085-1087.

[22]. Byun, K. M., Kim, S. J., & Kim, D. (2005). Design study of highly sensitive nanowire-enhanced surface plasmon resonance biosensors using rigorous coupled wave analysis. *Optics express*, *13*(10), 3737-3742.

[23]. Kim, K., Yoon, S. J., & Kim, D. (2006). Nanowire-based enhancement of localized surface plasmon resonance for highly sensitive detection: a theoretical study. *Optics Express*, *14*(25), 12419-12431.

[24]. Byun, K. M., Yoon, S. J., Kim, D., & Kim, S. J. (2007). Experimental study of sensitivity enhancement in surface plasmon resonance biosensors by use of periodic metallic nanowires. *Optics letters*, *32*(13), 1902-1904.

[25]. Malic, L., Cui, B., Veres, T., & Tabrizian, M. (2007). Enhanced surface plasmon resonance imaging detection of DNA hybridization on periodic gold nanoposts. *Optics letters*, *32*(21), 3092-3094.

[26]. Wu, S. Y., Ho, H. P., Law, W. C., Lin, C., & Kong, S. K. (2004). Highly sensitive differential phase-sensitive surface plasmon resonance biosensor based on the Mach–Zehnder configuration. *Optics Letters*, *29*(20), 2378-2380.

[27]. Markowicz, P. P., Law, W. C., Baev, A., Prasad, P. N., Patskovsky, S., & Kabashin, A. V. (2007). Phase-sensitive time-modulated surface plasmon resonance polarimetry for wide dynamic range biosensing. *Optics express*, *15*(4), 1745-1754.

[28]. Arakawa, E. T., Williams, M. W., Hamm, R. N., & Ritchie, R. H. (1973). Effect of damping on surface plasmon dispersion. *Physical Review Letters*, *31*(18), 1127.

[29]. Alexander, R. W., Kovener, G. S., & Bell, R. J. (1974). Dispersion curves for surface electromagnetic waves with damping. *Physical Review Letters*, *32*(4), 154.

[30]. Wang, S., Sun, X., Ding, M., Peng, G., Qi, Y., Wang, Y., & Ren, J. (2018). The investigation of an LSPR refractive index sensor based on periodic gold nanorings array. *Journal of Physics D: Applied Physics*, *51*(4), 045101.

[31]. Thamm, S., Csaki, A., & Fritzsche, W. (2018). LSPR Detection of Nucleic Acids on Nanoparticle Monolayers. In *DNA Nanotechnology* (pp. 163-171). Humana Press, New York, NY.

[32]. Oh, Y., Lee, W., & Kim, D. (2011). Colocalization of gold nanoparticle-conjugated DNA hybridization for enhanced surface plasmon detection using nanograting antennas. *Optics letters*, *36*(8), 1353-1355.

[33]. Moon, S., Kim, D. J., Kim, K., Kim, D., Lee, H., Lee, K., & Haam, S. (2010). Surface-enhanced plasmon resonance detection of nanoparticle-conjugated DNA hybridization. *Applied optics*, *49*(3), 484-491.

[34]. Hoa, X. D., Kirk, A. G., & Tabrizian, M. (2009). Enhanced SPR response from patterned immobilization of surface bioreceptors on nano-gratings. *Biosensors and Bioelectronics*, *24*(10), 3043-3048.

[35]. Ma, K., Kim, D. J., Kim, K., Moon, S., & Kim, D. (2010). Target-localized nanograting-based surface plasmon resonance detection toward label-free molecular biosensing. *IEEE Journal of Selected Topics in Quantum Electronics*, *16*(4), 1004-1014.

[36]. Gerdon, A. E., Oh, S. S., Hsieh, K., Ke, Y., Yan, H., & Soh, H. T. (2009). Controlled delivery of DNA origami on patterned surfaces. *small*, *5*(17), 1942-1946.

[37]. Homola, J., Yee, S. S., & Gauglitz, G. (1999). Surface plasmon resonance sensors. *Sensors and Actuators B: Chemical*, *54*(1-2), 3-15.

[38]. Sherry, L. J., Chang, S. H., Schatz, G. C., Van Duyne, R. P., Wiley, B. J., & Xia, Y. (2005). Localized surface plasmon resonance spectroscopy of single silver nanocubes. *Nano letters*, *5*(10), 2034-2038.

[39]. Lee, H. J., Wark, A. W., & Corn, R. M. (2008). Enhanced bioaffinity sensing using surface plasmons, surface enzyme reactions, nanoparticles and diffraction gratings. *Analyst*, *133*(5), 596-601.

[40]. Kim, S. A., Byun, K. M., Kim, K., Jang, S. M., Ma, K., Oh, Y., ... & Kim, S. J. (2010). Surface-enhanced localized surface plasmon resonance biosensing of avian influenza DNA hybridization using subwavelength metallic nanoarrays. *Nanotechnology*, *21*(35), 355503.

[41]. Cooper, M. A. (2003). Label-free screening of bio-molecular interactions. *Analytical and bioanalytical chemistry*, *377*(5), 834-842.

[42]. Hu, W. P., Chen, S. J., Huang, K. T., Hsu, J. H., Chen, W. Y., Chang, G. L., & Lai, K. A. (2004). A novel ultrahigh-resolution surface plasmon resonance biosensor with an Au nanocluster-embedded dielectric film. *Biosensors and Bioelectronics*, *19*(11), 1465-1471.

[43]. Sepúlveda, B., Angelomé, P. C., Lechuga, L. M., & Liz-Marzán, L. M. (2009). LSPR-based nanobiosensors. *Nano today*, *4*(3), 244-251.

[44]. Leong, H. S., Guo, J., Lindquist, R. G., & Liu, Q. H. (2009). Surface plasmon resonance in nanostructured metal films under the Kretschmann configuration. *Journal of applied physics*, *106*(12), 124314.

[45]. Rytov, S. M. (1956). Fluctuations in Oscillating Systems of the Thomson Type. II. *SOVIET PHYSICS JETP*, *2*(2).

[46]. Elser, J., Podolskiy, V. A., Salakhutdinov, I., & Avrutsky, I. (2007). Nonlocal effects in effective-medium response of nanolayered metamaterials. *Applied physics letters*, *90*(19), 191109.

[47]. Elser, J., Wangberg, R., Podolskiy, V. A., & Narimanov, E. E. (2006). Nanowire metamaterials with extreme optical anisotropy. *Applied physics letters*, *89*(26), 261102.

[48]. Hoa, X. D., Tabrizian, M., & Kirk, A. G. (2009). Rigorous coupled-wave analysis of surface plasmon enhancement from patterned immobilization on nanogratings. *Journal of sensors*, *2009*.

[49]. Cooper, M. A. (2002). Optical biosensors in drug discovery. *Nature reviews Drug discovery*, *1*(7), 515.

[50]. Oh, S., Moon, J., Kang, T., Hong, S., & Yi, J. (2006). Enhancement of surface plasmon resonance (SPR) signals using organic functionalized mesoporous silica on a gold film. *Sensors and Actuators B: Chemical*, *114*(2), 1096-1099.

[51]. Yuan, J., Oliver, R., Li, J., Lee, J., Aguilar, M., & Wu, Y. (2007). Sensitivity enhancement of SPR assay of progesterone based on mixed self-assembled monolayers using nanogold particles. *Biosensors and Bioelectronics*, *23*(1), 144-148.

[52]. Lyon, L. A., Musick, M. D., & Natan, M. J. (1998). Colloidal Au-enhanced surface plasmon resonance immunosensing. *Analytical chemistry*, *70*(24), 5177-5183.

[53]. Lyon, L. A., Holliway, W. D., & Natan, M. J. (1999). An improved surface plasmon resonance imaging apparatus. *Review of scientific instruments*, *70*(4), 2076-2081.

[54]. Raether, H. (1988). Surface plasmons on smooth surfaces. In *Surface plasmons on smooth and rough surfaces and on gratings* (pp. 4-39). Springer, Berlin, Heidelberg.

[55]. Haes, A. J., & Van Duyne, R. P. (2004). A unified view of propagating and localized surface plasmon resonance biosensors. *Analytical and bioanalytical chemistry*, *379*(7-8), 920-930.

[56]. Stuart, D. A., Haes, A. J., Yonzon, C. R., Hicks, E. M., & Van Duyne, R. P. (2005, February). Biological applications of localised surface plasmonic phenomenae. In *IEE Proceedings-Nanobiotechnology* (Vol. 152, No. 1, pp. 13-32). IET Digital Library.

[57]. Hu, X. L., Sun, L. B., Shi, B., Ye, M., Xu, Y., Wang, L. S., ... & Tai, R. Z. (2014). Influence of film thickness and nanograting period on color-filter behaviors of plasmonic metal Ag films. *Journal of Applied Physics*, *115*(11), 113104.

[58]. Landis, S., Brianceau, P., Reboud, V., Chaix, N., Désières, Y., & Argoud, M. (2013). Metallic colour filtering arrays manufactured by nanoimprint lithography. *Microelectronic Engineering*, *111*, 193-198.

[59]. Boltasseva, A., Bozhevolnyi, S. I., Søndergaard, T., Nikolajsen, T., & Leosson, K. (2005). Compact Z-add-drop wavelength filters for long-range surface plasmon polaritons. *Optics express*, *13*(11), 4237-4243.

[60]. Volkov, V. S., Bozhevolnyi, S. I., Devaux, E., Laluet, J. Y., & Ebbesen, T. W. (2007). Wavelength selective nanophotonic components utilizing channel plasmon polaritons. *Nano letters*, *7*(4), 880-884.

[61]. Laux, E., Genet, C., Skauli, T., & Ebbesen, T. W. (2008). Plasmonic photon sorters for spectral and polarimetric imaging. *Nature Photonics*, *2*(3), 161.

[62]. Ebbesen, T. W., Lezec, H. J., Ghaemi, H. F., Thio, T., & Wolff, P. A. (1998). Extraordinary optical transmission through sub-wavelength hole arrays. *Nature*, *391*(6668), 667.

[63]. Genet, C., & Ebbesen, T. W. (2010). Light in tiny holes. In *Nanoscience And Technology: A Collection of Reviews from Nature Journals* (pp. 205-212).

[64]. Maier, S. A. (2007). *Plasmonics: fundamentals and applications*. Springer Science & Business Media.

[65]. Yoon, K. H., Shuler, M. L., & Kim, S. J. (2006). Design optimization of nano-grating surface plasmon resonance sensors. *Optics express*, *14*(11), 4842-4849.

[66]. Awang, R. A., El-Gohary, S. H., Kim, N. H., & Byun, K. M. (2012). Enhancement of field–analyte interaction at metallic nanogap arrays for sensitive localized surface plasmon resonance detection. *Applied optics*, *51*(31), 7437-7442.

[67]. Tahmasebpour, M., Bahrami, M., & Asgari, A. (2014). Design study of nanograting-based surface plasmon resonance biosensor in the near-infrared wavelength. *Applied optics*, *53*(7), 1449-1458.